ILLINOIS

UNIVERSITY OF ILLINOIS AT URBANA-CHAMPAIGN

-

PRODUCTION NOTE

University of Illinois at
Urbana-Champaign Library
Large-scale Digitization Project, 2007.

UNIVERSITY OF ILLINOIS ENGINEERING EXPERIMENT STATION BULLETIN NO. 448

Inelastic Behavior of Aluminum Alloy I-Beams with Web Cutouts

by

Will J. Worley

UNIVERSITY OF ILLINOIS BULLETIN

A REPORT OF AN INVESTIGATION

Conducted by

THE ENGINEERING EXPERIMENT STATION

UNIVERSITY OF ILLINOIS

In Cooperation with

WRIGHT AIR DEVELOPMENT CENTER,
DEPARTMENT OF THE AIR FORCE

Price: One dollar

UNIVERSITY OF ILLINOIS BULLETIN

Volume 55, Number 62; April, 1958. Published seven times each month by the University of Illinois. Entered as second-class matter December 11, 1912, at the post office at Urbana, Illinois, under the Act of August 24, 1912. Office of Publication, 2 Administration Building (East), Urbana, Ill.

Inelastic Behavior of Aluminum Alloy I-Beams with Web Cutouts

by

Will J. Worley

ASSOCIATE PROFESSOR OF THEORETICAL AND APPLIED MECHANICS

ENGINEERING EXPERIMENT STATION BULLETIN NO. 448

2550—64947

UNIVERSITY
OF ILLINOIS
PRESS

ABSTRACT

This report attempts to answer the question, "What shape web-section cutout results in the least reduction in fully-plastic load-carrying capacity per pound of beam weight?" The process used in arriving at a partial solution is outlined below.

Data are presented on the elastic and fully-plastic behavior of 6061-T6 aluminum alloy I-beams with various cutout configurations. A sufficiently large number of tests were conducted using I-beams with rectangular- and elliptical-shape web-section cutouts to establish the validity of the mechanism method of analysis. The Upper Bound Theorem was used to predict the fully-plastic loads. These tests included both pure bending and center loading with various cutout lengths and spacings. The results indicated that for a pure bending load there was little difference between the fully-plastic strength of I-beams with rectangular cutouts and with elliptical cutouts. For center loading, the elliptical cutouts were much stronger.

The tests permitted the formulation of the failure mechanism in mathematical form suitable for programming on the ILLIAC digital computer. A series of cutout shapes were then investigated for a particular center-loaded I-beam of fixed length with one cutout in each half span. The equation defining the cutout is expressed as

$$\left(\frac{\pm u}{a}\right)^{\alpha}+\left(\frac{\pm v}{b}\right)^{\beta}=1$$

where u and v are the coordinates of the elliptic-type curves, a and b represent the major and minor axes, and α and β are the variable exponents which determine the shape of the cutout.

The ILLIAC results predicted that $\alpha=\beta=1$, or a diamond-shape cutout, would yield the greatest load-carrying capacity per pound of beam weight. This result was verified by experiment for both 3-in. and 6-in. depth 6061-T6 aluminum alloy I-beams.

CONTENTS

FIGURES

FIGURES (Continued)

TABLES

I. INTRODUCTION

In the design of various structures it is desirable to be able to predict the fully-plastic load carrying capacity of structural elements such as I-beams. This knowledge permits a more precise evaluation of the safety factor of the various components.

It is frequently necessary to have web-section cutouts in I-beams. These holes may be for access or to allow the passage of electrical cables, air ducts, etc.

Many reports are available which discuss the elastic behavior of various structural forms containing access holes of different shapes (see items 1 through 17 of the Bibliography). Recent emphasis, however, has been placed on investigations of the effect of inelastic action on the resistance of structural members to various types of loads. Experimental data on the behavior of structural members with access holes when loaded inelastically are rather limited.

Failure theories have been developed which make possible the relatively accurate prediction of the inelastic load-carrying capacity of members. According to Neal,[1]* apparently the first paper on the inelastic design of engineering structures was published by G. Kazinczy in Hungary in 1914. In 1940, J. A. van den Broek published a paper in the United States. The methods of calculating fully-plastic collapse loads for complex structures were not placed on a sound mathematical basis until 1949. At that time H. J. Greenberg and W. Prager stated and proved the basic principles for calculating the fully-plastic collapse load. This material was published in 1952.[2]

Engineering design requires a careful correlation of theory and experiment. When an inelastic theory is available, it is necessary to conduct sufficient tests to insure that the theory applies to the particular material and geometry under consideration. There are, however, far more compelling reasons for conducting experiments on beams with various cutout configurations. The prediction of the deflections by inelastic theories is quite difficult. The experimental results, on the other hand, yield both elastic and inelastic load-deflection behavior. The tests also reveal the various modes of failure not predicted by the inelastic theory, such as instability behavior or fracture. These modes of failure are beyond the scope of the inelastic or fully-plastic analysis, which assumes the development of ideal, fully-plastic hinges.

However, the methods of fully-plastic analysis served a useful purpose and were relied upon in predicting desirable cutout contours in this study. The predicted failure loads were verified by experimental results for the most promising case.

1. Object and Scope of Investigation

The object of this investigation was to study the effects of various web-section cutouts on the elastic and inelastic load-carrying capacity of aluminum alloy I-beams. Some beams were loaded with center loading which caused combined shear and bending. Other beams were loaded in pure bending.

The report attempts to answer the question, "What shape cutout results in the least reduction in fully-plastic load carrying capacity per pound of beam weight?"

This study was confined to one particular aluminum alloy which exhibited relatively flat static tension and compression stress-strain diagrams in the inelastic region, as well as high ductility. Tests were first conducted with rectangular web-section cutouts. The experimental results were then compared with the Upper Bound Theorem procedure for predicting the fully-plastic load-carrying capacity of the members. After establishing that the

* Superscripts in parentheses refer to corresponding entries in the list of References.

analysis was in agreement with the experimental data, elliptical cutouts were studied.

Tests with the elliptical cutout were conducted with different ratios of shear to moment loading. This variable was introduced for center-loaded beams by changing the length of the span for a given depth beam.

Following verification of the Upper Bound Theorem as a sufficiently accurate method of predicting the fully-plastic load-carrying capacity for both rectangular and elliptical web-section cutouts, the theory was extended to include a general elliptic-type curve. This study was confined to I-beams which had one cutout on either end of the beam. The equations were developed and programmed for the University of Illinois electronic digital computer, the ILLIAC. This phase of the project was intended to aid in answering the question concerning the cutout shape which results in the least reduction in the fully-plastic load-carrying capacity per pound of beam weight. Following this phase of the project, experimental tests were used to substantiate the ILLIAC results for the best cutout configuration.

2. Acknowledgments

The research was conducted in the Department of Theoretical and Applied Mechanics, Professor T. J. Dolan, Head. It was performed under the University of Illinois Engineering Experiment Station, W. L. Everitt, Director, in cooperation with the Wright Air Development Center under USAF Contract No. AF 33(616) 2753. Professor James O. Smith was project supervisor and Captain E. Dirkes acted as WADC project engineer. Dr. A. J. Herzog later assumed these duties. Dr. Shuji Taira assisted with the early phases of this project. Some of the material tested was donated by the Aluminum Company of America, Pittsburgh, Pennsylvania.

The assistance of the following graduate students, Donald L. Bitzer, who programmed the problems for solution on the ILLIAC, and James R. Young, who assisted with early phases of the test program and with the analysis of the results, is also gratefully acknowledged, as is the aid of student assistants F. D. Breuer, K. J. Castle, and R. E. Ruble. Other student assistants on the project were B. D. Elliott, K. W. Heid, R. S. Karaken, and F. J. Spokas.

II. ILLIAC PROGRAMMING AND RESULTS

3. Failure Theory

The failure mechanism was determined by observing the failure of I-beams with rectangular web-section cutouts and with elliptical web-section cutouts.[4, 5, 6] A comparison was made between the experimental load and the load obtained using the Upper Bound Theorem procedure of analysis.[1, 2, 3] It was then decided to use the simplest beam configuration to determine the cutout shape which would yield the greatest fully-plastic load-carrying capacity per pound of beam weight. The nature of the I-beam geometry which was selected appears in Fig. 1, where the shape of the cutout and the shape of the I-beam flange are shown, along with a number of the terms used in the analysis.

An extensive treatment of the mechanism method of analysis using the Upper Bound Theorem has been presented by Neal.[1] He states, "The method is to examine all possible collapse mechanisms, writing down the work equation for each mechanism and thus deriving the corresponding value of the collapse load. The actual value of the collapse load will then be the smallest value thus obtained. . . ." This procedure establishes an upper bound for the load.

A simple example, Fig. 2a, shows the failure mechanism for a rectangular cross-section cantilever beam of varying depth. This figure will be used to illustrate the procedure by which the theorem may be applied. First, it is assumed that a fully-plastic hinge will form at some distance, l from the load, $P/2$. The relation for the work done by the load during a virtual linear displacement, $l\delta\theta$, is then equated to the work done by the fully-plastic hinge moment, M_p, during the corresponding virtual angular displacement, $\delta\theta$. Thus $(P/2)l\delta\theta = M_p\delta\theta$. Since the beam is tapered, the hinge location, l, is initially unknown. Several trials would be necessary to establish the hinge location leading to a cross-section and deformation geometry which would result in a minimum load. For small angles, the virtual displacements may be replaced by the actual displacements since the geometric relations are essentially linear. This principle can be extended to more complex geometric configurations, such as Fig. 2b.

While the actual I-beams considered were loaded as simple beams with a concentrated load at the midspan, they may be represented as cantilever beams fixed at the center and having an upward

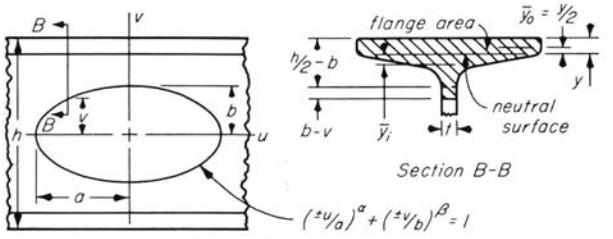

Fig. 1. I-Beam Geometry

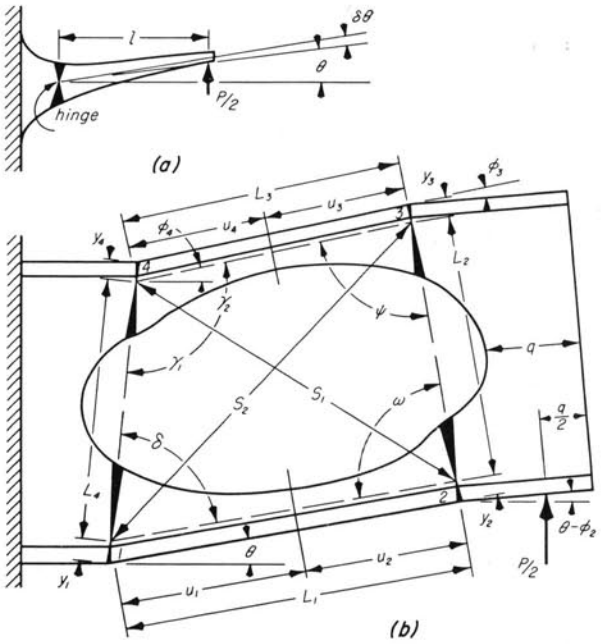

Fig. 2. Beam Failure Mechanism

load applied at the end. The assumed failure mechanism, Fig. 2b, was thus represented by four fully-plastic hinges for each half of the simple beam. The geometric relations which apply to Fig. 2b are those of the usual four-link mechanism so familiar in machine design.

In programming the problem for solution on the ILLIAC, the hinge locations were not known, so initial hinge locations were read into the machine. The program routine proceeded to shift the hinge locations until minimum load was obtained, using the Upper Bound Theorem procedure. The hinges were shifted from the initial position in such a way as to minimize the resulting load, P. The sequence in the minimization process was to shift the lower left hinge, then the lower right, the upper right, and, last, the upper left hinge. In the process of performing the minimization, calculations were made to determine the area of the flange and the portion of the web corresponding to a particular location along the elliptic-type curve $\left(\frac{\pm u}{a}\right)^{\alpha}+\left(\frac{\pm v}{b}\right)^{\beta}=1$. In the above equation, it was assumed that the sign of u and v would always be chosen so that the quantity was positive. In addition, the location of the fully-plastic neutral surface of section B-B, Fig. 1 was determined as well as the centroidal distances $\overline{y}_o$ and $\overline{y}_i$.

Although not used in this report, the Lower Bound Theorem may also be used in establishing inelastic failure loads. Neal[1] states this theorem as follows: "For a given frame and loading, if there exists any distribution of bending moment throughout the frame which is both safe and statically admissible with a set of loads W, the value of W must be less than or equal to the collapse load W_c."

4. Mathematical Relations

Most of the symbols used appear in Figs. 1 and 2b; the others will be defined as they arise. The equations presented contain the numerical values corresponding to the 6-in. I-beam.

The distance to the fully-plastic neutral surface, Fig. 1, for the flange and portion of the web of the 6-in. I-beam can be expressed as

$$y = 0.2933 - 0.0370v \tag{1}$$

Since the portion of the flange above the neutral surface was essentially rectangular, the centroid of this portion was expressed as

$$\overline{y}_o = y/2 = 0.1467 - 0.0185v \tag{2}$$

The centroid of the lower portion of the web and flange below the fully plastic neutral surface was determined as

$$\overline{y}_i = \frac{0.4297 - 0.2948v + 0.0543v^2}{0.4446 - 0.0575v} \tag{3}$$

The cutout geometry was expressed mathematically as

$$\left(\frac{\pm u}{a}\right)^{\alpha}+\left(\frac{\pm v}{b}\right)^{\beta}=1 \tag{4}$$

where it was understood that the $\pm$ sign was chosen so as to render $(\pm u)$ and $(\pm v)$ positive in all four quadrants. By means of the relation,

$$N^x = e^{x \ln N} \tag{5}$$

Equation 4 can be solved for v and expressed as

$$v = be^{\left(\frac{1}{\beta}\right) \ln [1-e^{\alpha \ln(u/a)}]} \tag{6}$$

Equation 4 in the form of Eq. 6 could be solved readily by means of a standard ILLIAC program.

From Figs. 2b and 4,

$$L_1 = u_1 + u_2 \tag{7}$$

$$L_3 = u_3 + u_4 \tag{8}$$

$$L_2^2 = (u_2 - u_3)^2 + (h - y_2 - y_3)^2 \tag{9}$$

$$L_4^2 = (u_1 - u_4)^2 + (h - y_1 - y_4)^2 \tag{10}$$

also

$$\delta = \delta_o - \theta = \frac{\pi}{2} - \theta - \tan^{-1}\left[\frac{u_1 - u_4}{\sqrt{L_4^2 - (u_1 - u_4)^2}}\right] \tag{11}$$

Equation 11, as well as Eqs. 13, 15, and 16, which follow, were written in terms of $\tan^{-1}$ since the ILLIAC could not be programmed to solve $\sin^{-1}$ or $\cos^{-1}$ readily. S_1 was expressed as

$$S_1^2 = L_1^2 + L_4^2 - 2L_1L_4 \cos \delta \tag{12}$$

The angle γ was defined as

$$\gamma = \gamma_1 + \gamma_2 = \sin^{-1}\left[\frac{L_1 \sin \delta}{S_1}\right] + \cos^{-1}\left[\frac{S_1^2 + L_3^2 - L_2^2}{2L_3S_1}\right]$$

$$\gamma = \gamma_1 + \gamma_2 = \frac{\pi}{2} - \tan^{-1}\left[\frac{S_1^2 + L_4^2 - L_1^2}{\sqrt{4L_4^2S_1^2 - (S_1^2 + L_4^2 - L_1^2)^2}}\right] + \tan^{-1}\left[\frac{\sqrt{4L_3^2S_1^2 - (S_1^2 + L_3^2 - L_2^2)^2}}{S_1^2 + L_3^2 - L_2^2}\right] \tag{13}$$

S_2 was expressed as

$$S_2^2 = L_3^2 + L_4^2 - 2L_3L_4 \cos \gamma \tag{14}$$

Using the above relations, the hinge angles were computed with $\phi_1 = \theta = 0.1$ radian, an arbitrary value which approximates the actual measurements for the beams. Likewise, using the transformation from $\cos^{-1}$ to $\tan^{-1}$ as in Eq. 13,

$$\phi_2 = |\omega_o - \omega| = \left|\tan^{-1}\left[\frac{u_2 - u_3}{\sqrt{L_2^2 - (u_2 - u_3)^2}}\right] - \tan^{-1}\left[\frac{L_1^2 + L_2^2 - S_2^2}{\sqrt{4L_1^2L_2^2 - (L_1^2 + L_2^2 - S_2^2)^2}}\right]\right| \quad (15)$$

$$\phi_3 = |\psi_o - \psi| = \left|\tan^{-1}\left[\frac{u_2 - u_3}{\sqrt{L_2^2 - (u_2 - u_3)^2}}\right] + \tan^{-1}\left[\frac{L_2^2 + L_3^2 - S_1^2}{\sqrt{4L_2^2L_3^2 - (L_2^2 + L_3^2 - S_1^2)^2}}\right]\right| \quad (16)$$

$$\phi_4 = |\gamma_o - \gamma| = |\gamma + \delta - \pi| \quad (17)$$

In Eqs. 11, 15, 16, and 17 the O subscript indicates the magnitude of the angle in the undeformed position. In addition to Eqs. 11 through 17, the following equation was used.

$$A_{fT} = \text{Flange area plus web area} = A_f + t(b - v) = 1.3077 + 0.23(2.25 - v) \quad (18)$$

where A_f is the flange cross-sectional area at $u = 0$ and $t(b - v)$ is the web cross-sectional area added as shown by Fig. 1.

When the work done by the four fully-plastic hinges is equated to the work done by the load, $P/2$, the following relation results,

$$\frac{P}{2}\left[L_1\theta + \left(a + \frac{q}{2} - u_2\right)(\theta - \phi_2)\right] = \sigma\sum_{n=1}^{n=4}\left[\phi_n \frac{A_{fT_n}}{2}(\bar{y}_0 + \bar{y}_i)_n\right] \quad (19)$$

where n denotes a particular hinge and σ is the average of the tensile and compressive fully-plastic strength as shown in Table 3. The values were $\sigma = 46{,}100$ psi and 42,300 psi, for the 3-in. and 6-in. I-beams, respectively. The compressive values were obtained at an arbitrary deformation of 0.025 in. per in., for columns with flat ends having an l/r ratio of approximately 15.

The Upper Bound Theorem makes use of the principle that the work done by the external forces during a virtual linear displacement is equal to the work done by the internal moments during a virtual angular displacement. In developing Eq. 19 it was assumed that since the angular displacement ϕ_1 is very small, the virtual angular displacements of ϕ_2, ϕ_3, and ϕ_4 are essentially linear functions of the virtual angular displacement of ϕ_1. Thus the external work could be equated to the internal work.

Table 1

Static Tension and Compression Test Results

	Modulus of Elasticity, psi, x10^{-6}	Yield Strength 0.2% offset, psi	Ultimate Strength, psi	Elongation, %	Reduction of Area, %
Rectangular Cutouts					
3-in. I-Beam Tension Tests	10.20	40,200	43,100	15.5	46.6
	10.16	39,900	43,000	15.0	46.5
Compression Tests	10.47	39,100	44,600*	....	....
	10.46	38,800	44,300*	....	....
	10.39	39,000	44,300*	....	....
Tension and Compression Average	10.31	39,500	43,700	....	....
6-in. I-Beam Tension Tests	10.40	36,300	39,800	15.0	51.4
	10.25	36,000	39,600	16.5	50.5
Compression Tests	10.35	36,800	45,100*	....	....
	10.35	36,800	44,800*	....	....
	10.90	35,900	42,900*	....	....
	10.75	35,800	44,900*	....	....
Tension and Compression Average	10.48	36,300	42,100	....	....
Elliptical and Diamond-Shaped Cutouts					
3-in. I-Beam Tension Tests	10.7	39,800	45,800	16.0	42.4
	10.3	40,300	46,000	16.0	40.5
Compression Tests	10.8	39,900	45,700*	....	....
	10.5	39,900	46,900*	....	....
Tension and Compression Average	10.6	40,000	46,100	....	....
6-in. I-Beam Tension Tests	10.3	38,100	41,300	16.0	45.0
	10.0	37,800	41,700	18.0	49.5
Compression Tests	9.9	37,500	42,900*	....	....
	10.4	37,900	43,100*	....	....
Tension and Compression Average	10.2	37,800	42,300	....	....

* Compressive Ultimate Strength based on a deformation of 0.025 in./in. and specimen column ratio of approximately 15.

ILLIAC solutions were obtained with Eq. 19 in the form

$$\left(\frac{P}{\sigma}\right) = \frac{\sum_{n=1}^{n=4}\left[\phi_n \frac{A_{fT_n}}{2}(\bar{y}_o + \bar{y}_i)_n\right]}{L_1\theta + \left(a + \frac{q}{2} - u_2\right)(\theta - \phi_2)} \quad (20)$$

as illustrated in Table 4.

The ILLIAC results were in turn multiplied by σ and divided by the weight of the beam between the lower loading points. The following equations were used for determining the weights for the 3-in. and 6-in. I-beams, respectively.

$$W = (4a + 2q)w - 2\,(\text{Area of one cutout}) \cdot (t)\,(0.098\ \text{lb/in.}^3),\ \text{lb.} \quad (21)$$

For the 3-in. I-beam

$$a = 3.75\ \text{in.}, \quad q = 1.5\ \text{in.}, \quad w = 0.1633\ \text{lb/in.}, \quad t = 0.17\ \text{in.}, \quad W = 2.94 - 0.0333A_c,\ \text{lb} \quad (22)$$

where A_c is the area of the cutout.

For the 6-in. I-beam

$$a = 5.0\ \text{in.}, \quad q = 2\ \text{in.}, \quad w = 0.3583\ \text{lb/in.}, \quad t = 0.23\ \text{in.}, \quad W = 8.60 - 0.0451A_c,\ \text{lb.} \quad (23)$$

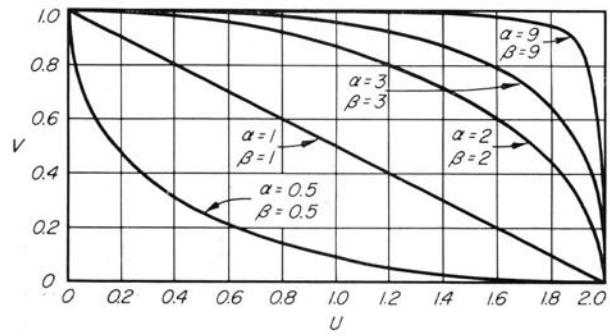

(a) Typical curves for $\alpha = \beta$

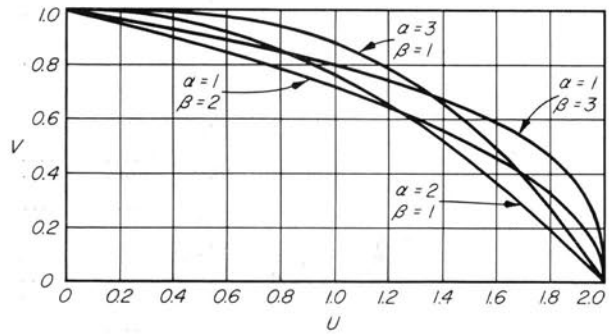

(b) Typical curves for $\alpha \neq \beta$

Fig. 3. Elliptic-Type Cutout Geometry for $\left(\frac{\pm u}{2}\right)^{\alpha} + \left(\frac{\pm v}{1}\right)^{\beta} = 1$

The area enclosed by Eq. 4 may be represented[7] by

$$A_c = 4ab\left[\frac{\Gamma\left(\frac{1}{\alpha}+1\right)\Gamma\left(\frac{1}{\beta}+1\right)}{\Gamma\left(\frac{1}{\alpha}+\frac{1}{\beta}+1\right)}\right] \qquad (24)$$

where $\Gamma(N) = (N-1)!$. The nature of Eq. 24 is such that an interchange of α and β yields the same area. Also, if α (or β) is equal to unity the equation becomes

$$A_{c_{\alpha=1}} = 4ab\left[\frac{\beta}{1+\beta}\right] \qquad (25)$$

$$A_{c_{\beta=1}} = 4ab\left[\frac{\alpha}{1+\alpha}\right] \qquad (26)$$

5. ILLIAC Results

Figure 3 indicates the shapes of some of the curves which were investigated. Figure 3a shows curves for $\alpha = \beta$ while Fig. 3b shows a few of the other curves for which values of P/W were obtained. In Fig. 3a the curve $\alpha = \beta = 0.5$ was presented to show a possible shape of cutout, but one which would be impractical because of high stress concentrations. In these figures $a = 2$ and $b = 1$, which does not correspond with the length to height ratio of either the 3-in. or the 6-in. I-beam cutouts. However, it is nearly the same as the 6-in. I-beam cutout which has a ratio of 2 to 0.9.

Table 2

ILLIAC Results for 3-In. I-Beams

All values apply for $a = 3.75$ in., $b = 0.875$ in., $(a + q/2) = 4.50$ in., $\theta = 0.1$ rad., $\sigma = 46{,}100$ psi.

α	β	u_1	u_2	u_3	u_4	% Wt Removed	P/W
1.0	1.0	3.68	3.68	3.16	2.56	7.44	3610
1.2	1.2	3.14	3.32	2.62	2.52	8.75	3360
1.5	1.5	2.90	3.04	2.58	2.40	10.18	2940
2.0	2.0	2.90	3.00	2.72	2.58	11.68	2490
2.5	2.5	3.00	3.08	2.84	2.74	12.57	2230
3.0	3.0	3.08	3.14	2.96	2.86	13.14	2060
6.0	6.0	3.36	3.38	3.30	3.26	14.34	1680
8.0	8.0	3.44	3.46	3.40	3.36	14.55	1590
9.0	9.0	3.48	3.50	3.42	3.40	14.62	1560
1.0	1.2	3.38	3.52	3.84	2.52	8.11	3470
1.0	1.5	3.16	3.28	2.80	2.56	8.93	3240
1.0	2.0	3.10	3.20	2.84	2.68	9.92	2920
1.0	2.5	3.12	3.22	2.92	2.78	10.62	2700
1.0	3.0	3.16	3.24	2.98	2.86	11.16	2530
1.5	1.0	2.94	3.24	2.52	2.52	8.93	3400
1.5	2.0	2.96	3.08	2.74	2.58	11.00	2670
1.5	2.5	3.04	3.12	2.84	2.72	11.57	2490
1.5	3.0	3.10	3.18	2.94	2.82	11.99	2360
2.0	1.0	2.60	2.80	2.52	2.52	9.92	3110
2.0	1.5	2.78	2.92	2.56	2.52	11.00	2720
2.0	2.5	3.00	3.08	2.84	2.72	12.16	2340
2.0	3.0	3.08	3.14	2.92	2.82	12.51	2230
2.5	1.0	2.54	2.68	2.52	2.52	10.62	2860
2.5	1.5	2.76	2.86	2.56	2.52	11.57	2540
2.5	2.0	2.90	2.98	2.72	2.62	12.16	2360
3.0	1.0	2.54	2.66	2.52	2.52	11.16	2670
3.0	1.5	2.76	2.86	2.60	2.52	11.99	2410
3.0	2.0	2.90	2.98	2.76	2.66	12.51	2250

Table 3

ILLIAC Results for 6-In. I-Beams

All values apply for $a = 5.00$ in., $b = 2.25$ in., $(a + q/2) = 6.00$ in., $\theta = 0.1$ rad., $\sigma = 42{,}300$ psi.

α	β	u_1	u_2	u_3	u_4	% Wt Removed	P/W
1.0	1.0	2.56	3.52	2.48	1.76	11.79	3870
1.5	1.5	2.64	2.98	2.64	2.30	15.88	2440
2.0	2.0	3.00	3.22	2.96	2.74	18.53	1880
2.5	2.5	3.28	3.44	3.24	3.08	19.94	1600
3.0	3.0	3.50	3.64	3.46	3.32	20.84	1430
6.0	6.0	4.18	4.24	4.14	4.08	22.73	1070
9.0	9.0	4.42	4.48	4.40	4.36	23.18	970
1.0	1.2	2.62	3.28	2.60	1.98	12.87	3280
1.0	1.5	2.78	3.26	2.74	2.22	14.15	3060
1.0	2.0	3.00	3.36	2.94	2.54	15.73	2610
1.0	2.5	3.20	3.48	3.12	2.80	16.85	2320
1.0	3.0	3.34	3.60	3.28	2.98	17.69	2120
1.5	1.0	2.22	2.66	2.28	1.92	14.15	2960
1.5	2.0	2.94	3.20	2.90	2.60	17.44	2160
1.5	2.5	3.16	3.38	3.10	2.84	18.34	1970
1.5	3.0	3.32	3.52	3.26	3.04	19.02	1830
2.0	1.0	2.34	2.64	2.38	2.08	15.73	2430
2.0	1.5	2.72	2.98	2.72	2.46	17.44	2090
2.0	2.5	3.20	3.40	3.16	2.96	19.28	1750
2.0	3.0	3.38	3.54	3.32	3.14	19.84	1640
2.5	1.0	2.50	2.72	2.50	2.28	16.85	2100
2.5	1.5	2.84	3.04	2.84	2.62	18.34	1860
2.5	2.0	3.10	3.28	3.06	2.88	19.28	1710
3.0	1.0	2.64	2.82	2.64	2.46	17.69	1890
3.0	1.5	2.96	3.12	2.94	2.78	19.02	1700
3.0	2.0	3.20	3.34	3.16	3.00	19.84	1580

The condition $\alpha = \beta = 1$ led to abrupt changes in cutout contour direction at $u = a$ and $v = b$, and thus to stress concentrations. However, the four-link failure mechanism model, with which the ILLIAC solutions were obtained, did not take these stress concentrations into account. The stress concentrations for $\alpha = \beta = 1$ were reduced by using radii at the points $u = a$ and $v = b$ for the test beam.

Stress concentrations which occur at abrupt changes in cross-section in the elastic range of

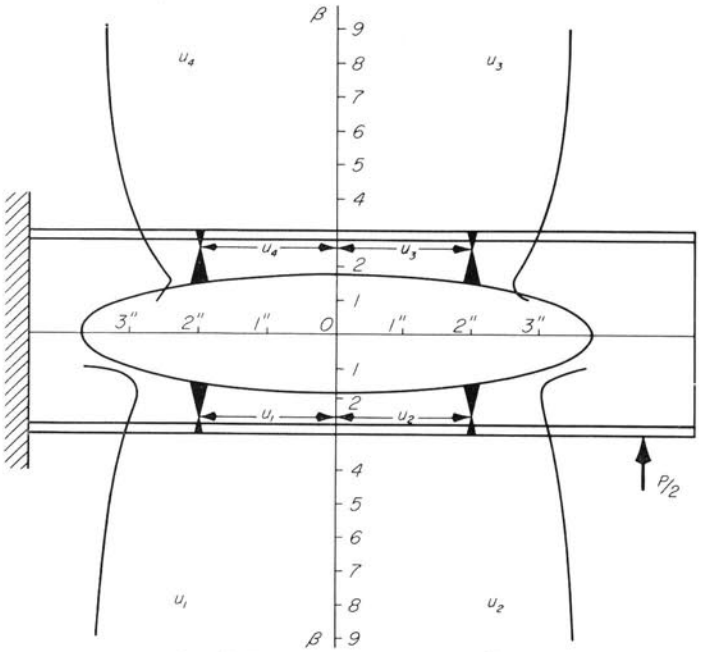

Fig. 4. Hinge Location with $\alpha = \beta$ for 3-in. I-Beams

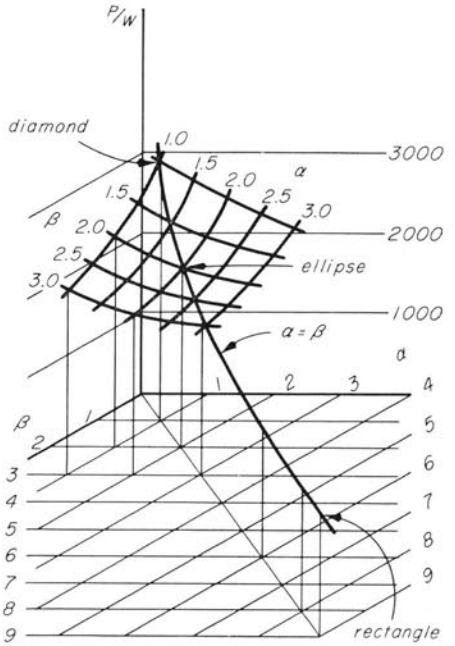

Fig. 5. Load Capacity vs. Cutout Geometry, 6061-T6, 3-in. I-Beams

stresses exist to a lesser degree in the inelastic range. These inelastic stress concentrations vary in importance with the ductility and yielding characteristics of the material. The more nearly ductile the material, the less significant their effect.

The ILLIAC solutions appear in Figs. 4 through 7. Figures 4 and 6 present the hinge location data for $\alpha = \beta$, and Figs. 5 and 7 present the values of P/W *vs.* α *vs.* β for the 3-in. and 6-in. I-beams, respectively. The data are also presented in Tables 2 and 3.

These are not general curves, but apply only to 6061-T6 aluminum alloy. It would be necessary to divide by the reported values of σ and multiply by the new values before these curves could be applied to another alloy. Even then it would have

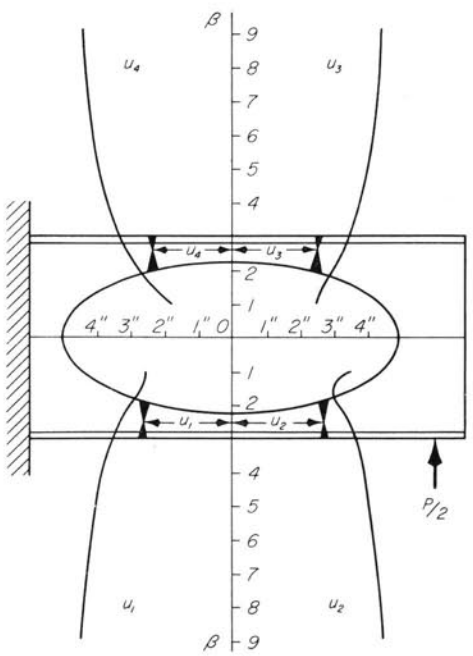

Fig. 6. Hinge Locations with $\alpha = \beta$ for 6-in. I-Beams

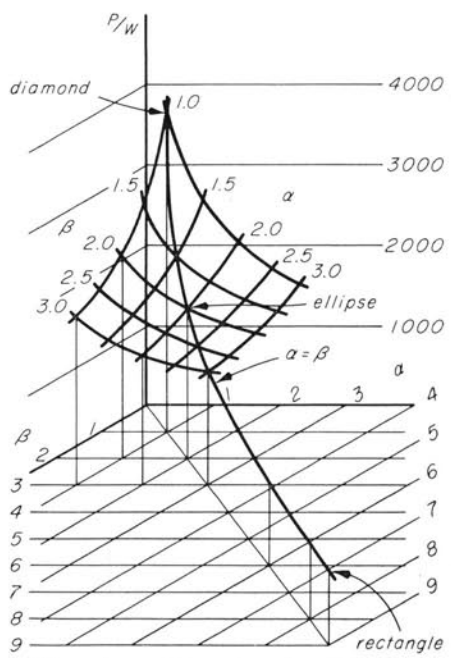

Fig. 7. Load Capacity vs. Cutout Capacity, 6061-T6, 6-in. I-Beams

Table 4

Determination of Maximum Load for 6-In. I-Beam No. 7-D-1

Hinge No.	1	2	3	4
u, average	3.00	3.34	2.05	3.18
v, average	0.90080	0.75620	1.34530	0.83480
0.28344	0.28344	0.28344	0.28344	0.28344
$0.03648v$	0.03286	0.02759	0.04908	0.03045
$y = 0.28344 - 0.03648v$	0.25058	0.25585	0.23436	0.25299
$\overline{y}_o = y/2$	0.12529	0.12793	0.11718	0.12650
v^2	0.81144	0.57184	1.80983	0.69689
$0.05407v^2$	0.04387	0.03092	0.09786	0.03768
0.43868	0.43868	0.43868	0.43868	0.43868
① $0.05407v^2 + 0.43868$	0.48255	0.46960	0.53654	0.47636
② $0.29465v$	0.26542	0.22281	0.39639	0.24597
③ ① + ②	0.21713	0.24679	0.14015	0.23039
0.46268	0.46268	0.46268	0.46268	0.46268
$0.05724v$	0.05156	0.04328	0.07700	0.04778
④ $0.46268 - 0.05724v$	0.41112	0.41940	0.38568	0.41490
$\overline{y}_i =$ ③/④	0.52814	0.58844	0.36338	0.55529
$(b - v) = (2.26 - v)$	1.35920	1.50380	0.91470	1.42520
$0.2288\,(b - v)$	0.31098	0.34407	0.20928	0.32609
A_f	1.34020	1.34020	1.34020	1.34020
$A_{fT_n} = A_f + 0.2288\,(b - v)$	1.65118	1.68427	1.54948	1.66629
$(\overline{y}_o + \overline{y}_i)_n$	0.65343	0.71637	0.48056	0.68179
$A_{fT_n}(\overline{y}_o + \overline{y}_i)_n$	1.07893	1.20656	0.74462	1.13606
Φ_n (radians)	0.07825	0.07250	0.08095	0.08595
$\Phi_n A_{fT_n}(\overline{y}_o + \overline{y}_i)_n$	0.08443	0.08748	0.06028	0.09764

$\sum_{n=1}^{n=4} \Phi_n A_{fT_n} (\overline{y}_o + \overline{y}_i)_n = 0.32983$

⑤ $(u_1 + u_2)\,\Phi_1 = (3.00 + 3.34)\,(0.07825) = 0.49611$

⑥ $[(a + q/2) - u_2]\,(\Phi_1 - \Phi_2) = (6.014 - 3.34)\,(0.07825 - 0.0725) = 0.01538$

Load Deflections $\Delta_{calculated} = \Delta_c = ⑤ + ⑥ = 0.51149$ in.

$$P = \frac{\sigma}{\Delta_c} \sum_{n=1}^{n=4} \left[\Phi_n A_{fT_n} (\overline{y}_o + \overline{y}_i)_n \right] = \frac{42{,}300}{0.51149} [0.32983] = 27{,}280 \text{ lb}$$

Load Deflection, $\Delta_{measured} = \Delta_m = 0.55$ in.

$$P = \frac{42{,}300}{\Delta_m} (0.32983) = \frac{42{,}300}{0.55} (0.32983) = 25{,}370 \text{ lb}$$

Measured beam depth = 6.02 in., $b = 2.26$ in.

to be established that the stress-strain curves had a relatively constant stress level in the yield region to comply with assumptions used in this analysis.

In Figs. 4 and 6 for $\alpha = \beta$, the hinges shift toward the center of the beam as $\alpha = \beta$ is reduced from 9 to 2. However, as the value of $\alpha = \beta$ decreases to 1.5 and to 1, the hinges again move out for the 3-in. I-beam and u_2 moves out at $\alpha = \beta = 1$ for the 6-in. I-beam. The results may be read more accurately from Tables 1 and 2.

In Figs. 5 and 7 it is seen that the condition $\alpha = \beta = 1$ yields the strongest beam per pound of weight of beam between the lower loading points. The diagonal line $\alpha = \beta$ includes all of the conditions for which tests have been conducted. The rectangle is closely approximated by $\alpha = \beta = 9$.

III. STATIC TENSION AND COMPRESSION TESTS

6. Material, Specimens, Apparatus, and Test Procedure

Aluminum alloy 6061-T6 was used for both the 3-in. and 6-in. I-beams. However, the 3-in. beams were rolled while the 6-in. beams were extruded. All 3-in. I-beams were designated as 1.96 pounds per foot with 0.17-in. web thickness, while all 6-in. I-beams were designated as 4.30 pounds per foot with 0.23-in. web thickness.

Standard static tension and compression test specimens were used as indicated in Fig. 8. The portions of the I-beam flange section from which the tension specimens were obtained for the investigation of elliptic and diamond-shape cutouts are shown. For the investigation of rectangular cutouts, the tension specimens were taken from the web section. The variation in tensile strength due to this difference in location is believed to be small. The compression test specimens were cut from the portion of the I-beam where the flange and web join in order to obtain a maximum test specimen diameter. The length to diameter ratio was maintained as nearly as practical at 4 to 1.

Templin wedge-grips and a 2-in. gage length were used in testing the tension specimens. The tests were conducted at 0.05 in. per min head speed.

The compression test apparatus was essentially the same as that described in ASTM Standards 1955, designation E9-52T. A 1-in. gage length was used and the head speed was 0.05 in. per min.

7. Test Results

The static tension and compression test results are summarized in Table 1. Both the static tension and compression yield-strength values were higher for the material used for the I-beams with elliptical and diamond cutouts. The same trend was observed for the ultimate strengths.

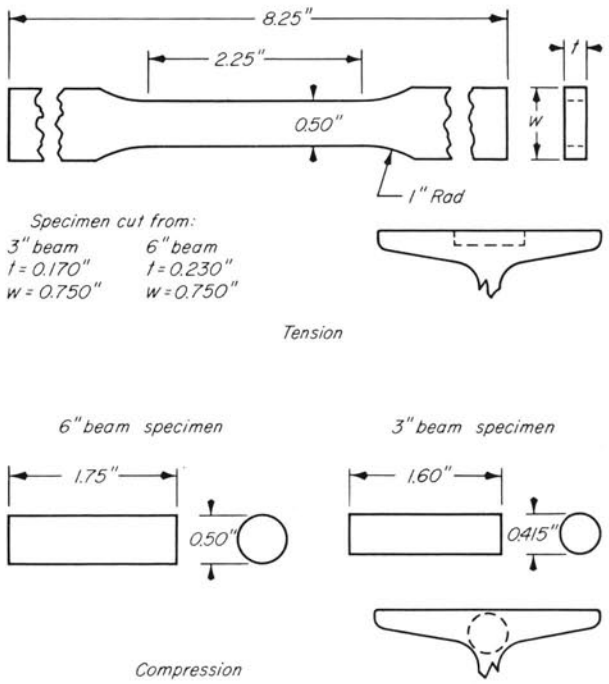

Fig. 8. Static Tension and Compression Test Specimens

The compressive "ultimate" strength reported in Table 1 was based on a deformation of 0.025 in. per in. While this value is arbitrary, its effect on the predicted load-carrying capacity is small. For example, at 0.04 in. per in. strain, the load sustained by the compression specimen was 3.5% greater than the value for 0.025 in. per in. strain.

The stress-strain diagrams for the static tension and compression tests appear in Figs. 9 and 10, respectively. The tension curves exhibit a relatively flat inelastic region. The compression curves, however, continue to rise because of the dilation of the specimen in compression.

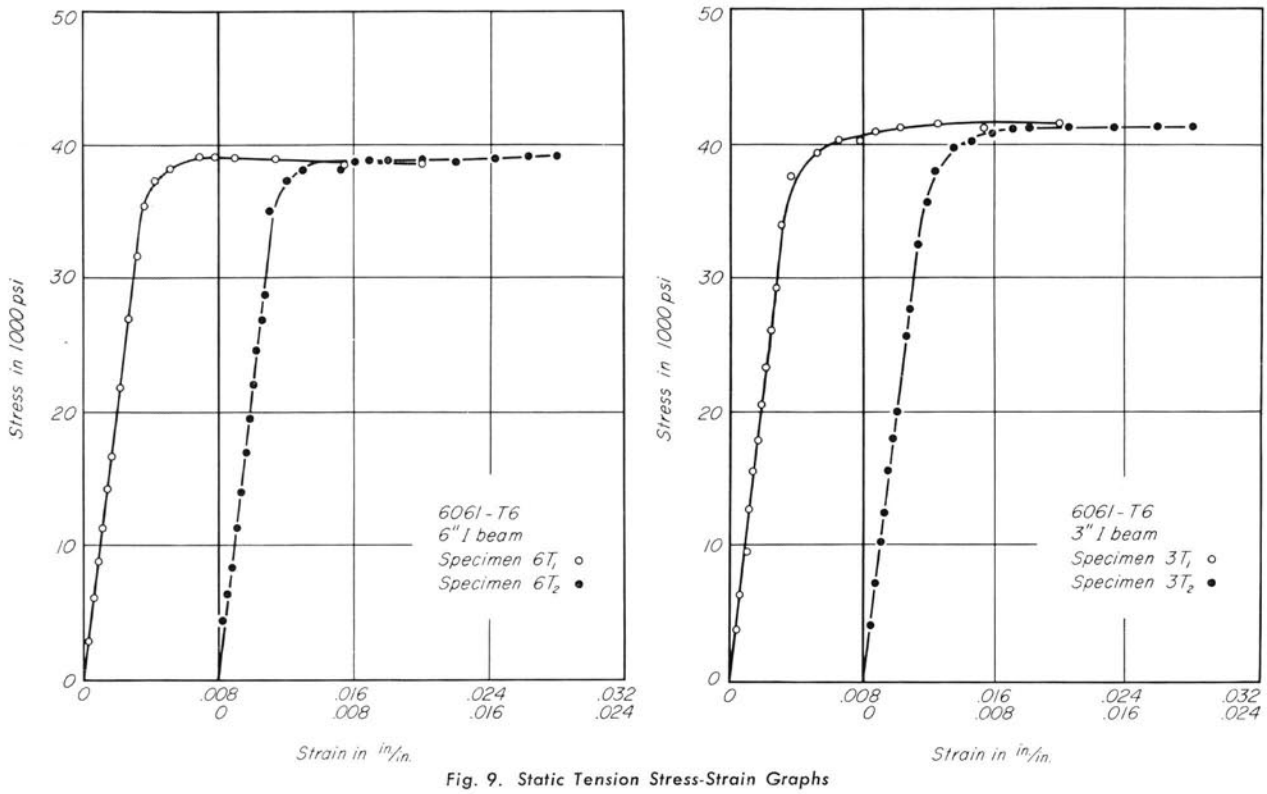

Fig. 9. Static Tension Stress-Strain Graphs

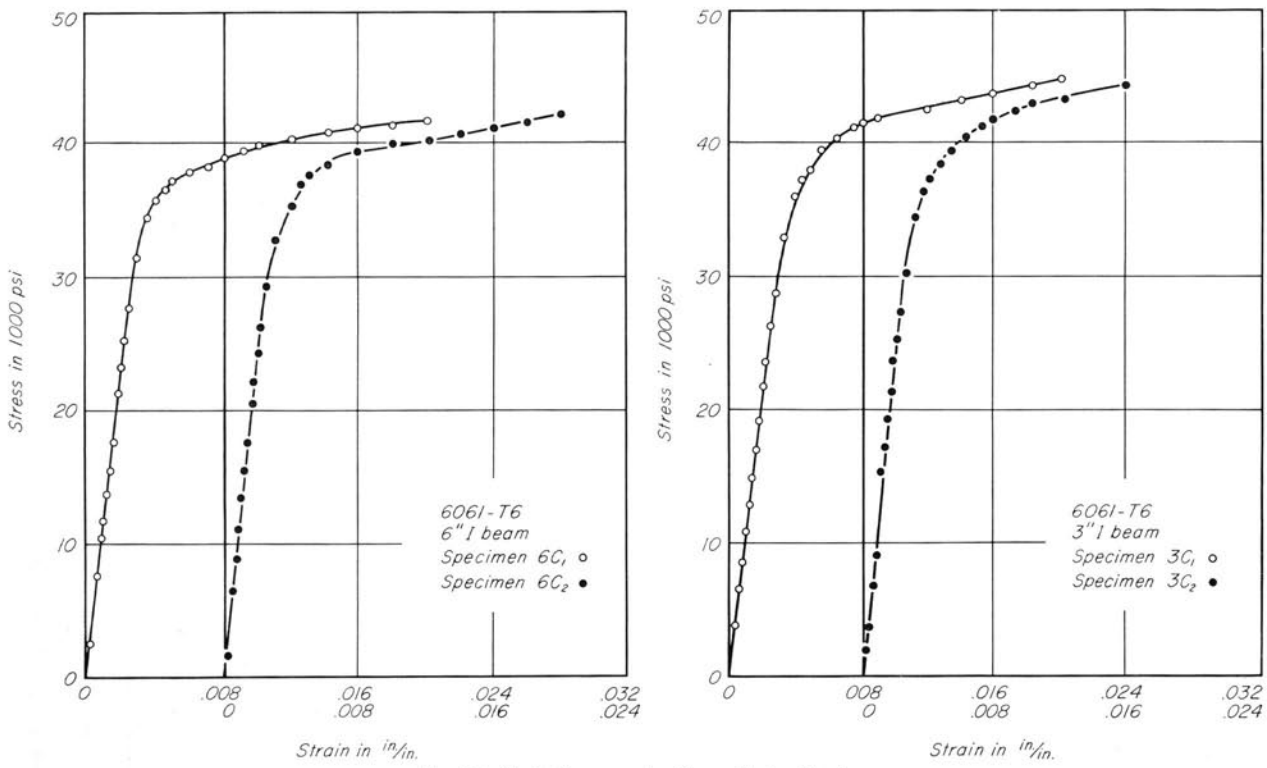

Fig. 10. Static Compression Stress-Strain Graphs

IV. BENDING TESTS

8. Specimens, Apparatus, and Test Procedure

All 3-in. I-beams had cutouts with a height of 1.75-in., while all 6-in. I-beams had cutouts with a height of 4.5-in. These heights were sufficient to remove the web section to the point at which the flange fillet radius began.

Beams were tested with rectangular, elliptical, and diamond-shape cutouts. The corner radii for the rectangular cutouts were 0.4375 in. and 0.5 in. for the 3-in. and 6-in. I-beams, respectively. These radii resulted in an elastic stress concentration factor of 1.2 or lower. The end radii used for the diamond-shape cutouts, which exhibited flange failures, were 0.0781 in. and 0.25 in. for the 3-in. and 6-in. I-beams, respectively. All cutouts were made on a milling machine.

The complete series of beam tests with elliptical web-section cutouts appears in Fig. 11. This figure shows a typical test program similar to the program conducted for rectangular cutouts. The beams with rectangular web-section cutouts appear in Figs. 15 through 25. The individual tests of beams with elliptical web-section cutouts appear in Figs. 26a through 28f while Fig. 36 shows the individual tests of beams with diamond-shape cutouts.

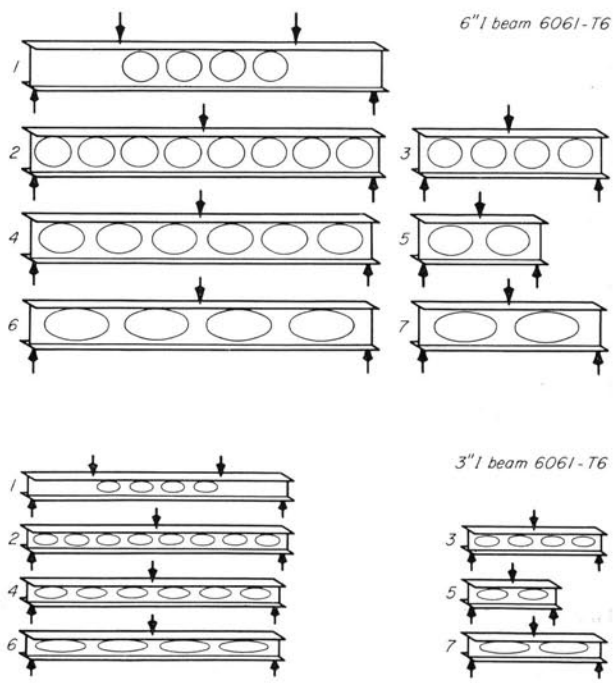

Fig. 11. Outline of Bending Test Program

A 200,000 lb Olsen universal testing machine, equipped with horizontal extensions on the weighing head, was used for all beam tests. The arrangement of the loading apparatus, dial gages, and lateral supports appears in Figs. 12, 13, and 14. Figure 12 shows the pure bending apparatus. The specimen was mounted on rollers at either end and at the quarter-points. A steel ball was used to transfer the load from the loading head to the loading beam. Dial gages were mounted at the center and quarter-points and one or two-dial bridges were attached to the beam to determine the deformation behavior over shorter spans. A front view of the apparatus used for center loading appears in Fig. 13. The lateral supports may be seen in the side view in Fig. 14. In order to reduce the effects of friction, the lateral supports were lubricated with SAE 30 oil for all beam tests.

The loading speed was 0.03 in. per min. In the range of load where pronounced yielding occurred, one to two minutes was allowed to lapse after each loading period before taking the load reading. This interval was sufficient for the entire beam to reach a nearly stable state where the rate at which the load was falling was negligible.

The 3-in. and 6-in. I-beams with elliptical and with diamond-shape web-section cutouts tested with center loading were coated with bluing dye and scribed with grid lines on the web sections using 0.10-in. spacing. These lines, which were initially straight, may be seen on the enlarged sections in Figs. 30 and 33. Figures 35 and 37 show the deformed grid lines for the diamond cutouts.

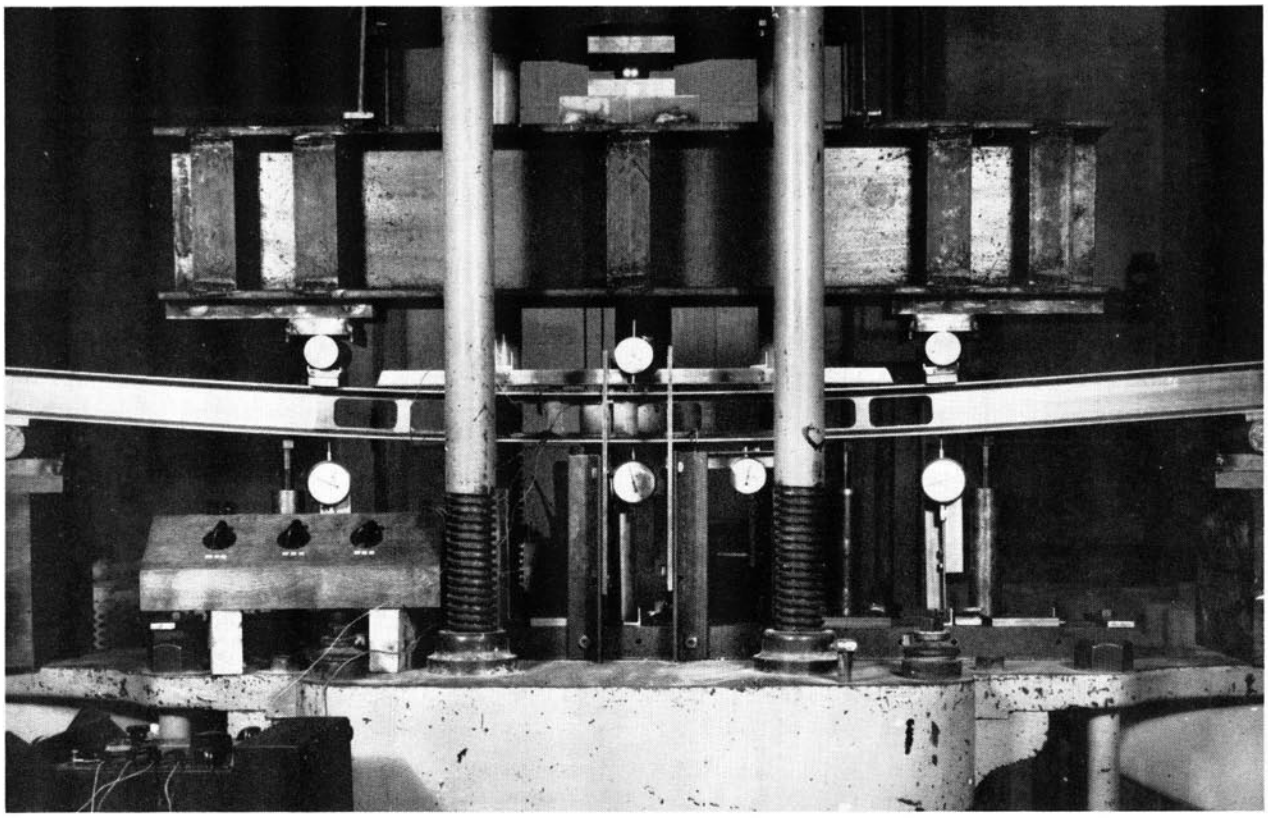

Fig. 12. Pure Bending Apparatus, Front View

The grid lines served two functions. They were used to establish coordinates for taking micrometer readings to determine the actual machined shape of the cutouts. For the ellipse, measurements were taken at 1.0, 0.5, 0.3, or 0.2-in. intervals, depending on the slope of the elliptical contours in the particular region. The other function of these grid lines was to establish an idea of the deformation behavior of the failure mechanism. This function is clearly seen in the enlargements. The lines were scribed to such a shallow depth that it was assumed they had very little effect on the ultimate load-carrying capacity or on the mode of failure of the various beams.

Tests were conducted with 3-in. and 6-in. I-beams having various lengths of cutouts and various widths of uprights. The uprights constituted the web material between adjacent cutouts. The I-beams of a given depth were proportioned so that the same weight of material per foot of beam length between loading points was removed from the web section for all of the cutout shapes in a given series. The weight reduction resulting from the removal of this material appears in Table 6 under the heading, *Weight Removed, %*.

The test program consisted of three major phases. First, rectangular, then elliptical, and last, diamond-shape web-section cutouts were investigated. The tests are discussed in this sequence.

9. Rectangular Cutouts — Pure Bending

The sections of the upper flange above the cutout failed by buckling under pure bending loads. Since the flange sections were partially fixed-end columns, it was necessary to establish an end-restraint factor, K. A thorough treatment of the behavior of columns with intermediate values of slenderness ratios and various end conditions has been presented by Shanley.[9] Calculations based on the failure load of 3-in. I-beam 2 indicated that the flange behaved as an Euler column. This flange was thus used as a reference to establish the factor K for 3-in. I-beams 3 and 5 as well as for 6-in. I-beam 1. The effective length, λ_e, of the flange section was taken as the cutout length, λ, minus twice the fillet radius, r, plus $2r \sin 15°$. That is, the effective length was assumed to be located 15° along the fillet on each end. This lead to the effective length relation, $\lambda_e = (\lambda - 1.48r)$. Using this effective length the value of K was calculated as

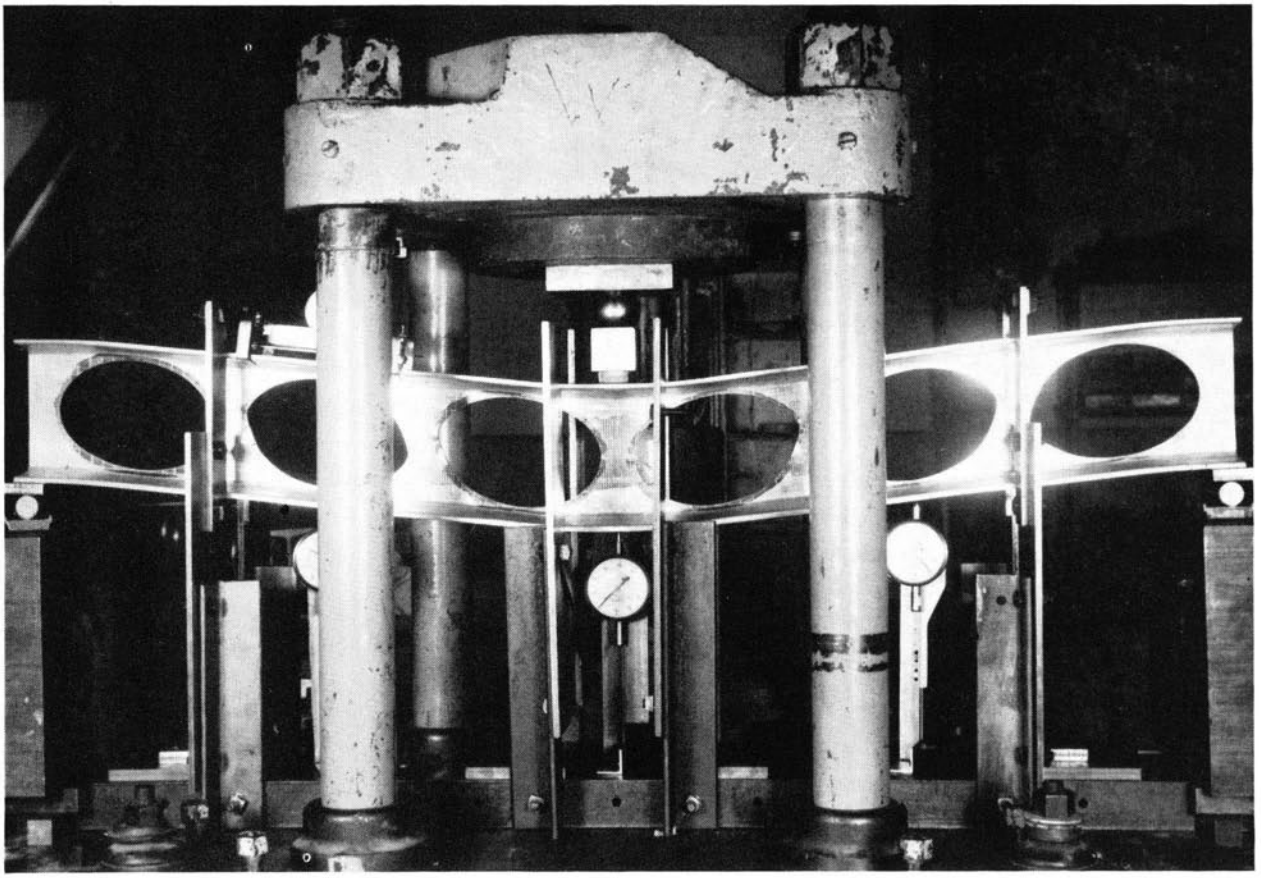

Fig. 13. Center Loading Apparatus, Front View

0.64. The tangent modulus column equation, obtained by replacing E by E_{tan} in the Euler column equation, was used in making load calculations for the other three I-beams. Values of E_{tan} were obtained from bulletin ANC-5.[10]

Because 3-in. I-beam 2 was used in computing K, the ultimate load reported in Table 5 agreed exactly with the ultimate test load. Reasonable agreement between the test load and the predicted load was indicated for 3-in. I-beams 3 and 5. Figure 19 shows the mode of failure of 3-in. beams. The test load for 6-in. I-beam 1 was substantially lower than the predicted load because the beam failed due to lateral instability and did not develop a true column failure in the upper flange.

The load-deflection behavior for the above

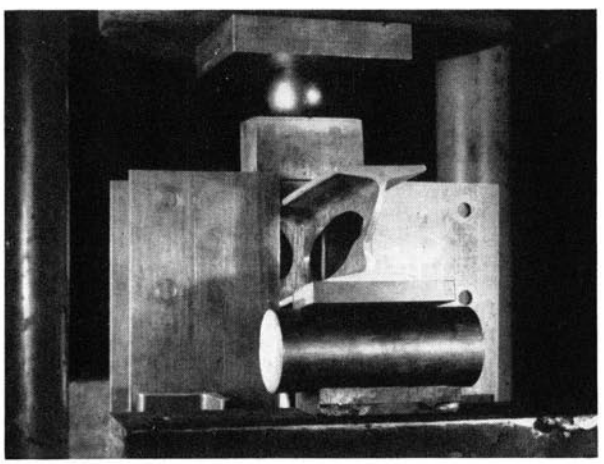

Fig. 14. Center Loading Apparatus, Side View

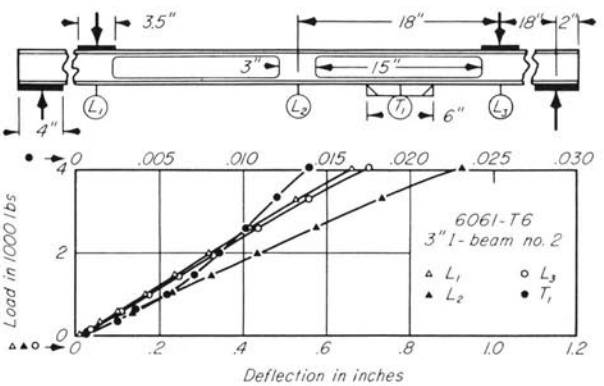

Fig. 15. Load-Deformation Behavior for 3-in. I-Beam No. 2, Rectangular Cutouts

Table 5

I-Beam Test Results

Beam No.	Proportional Limit Load, lb	Ultimate Load From Test, lb	Ultimate Load From, Theory, lb	Load (Ultimate / Prop. Limit), %	Mid-Point Deflection Prop. Limit Load, in.	Mid-Point Deflection Ultimate Load, in.	Deflection, (Ultimate / Prop. Limit), %
			Rectangular Cutouts				
3-in. No. 1	7,200	9,000	9,350	125	1.25	1.88	150
2	3,300	4,040	4,040	122	0.73	0.93	127
3	6,000	7,250	7,300	121	1.30	1.68	129
5	6,600	8,200	7,940	124	1.48	2.61	176
4B	1,100	3,230	3,350	294	0.26	1.89	727
7	1,550	3,190	3,200	206	0.20	1.68	840
6-in. No. 1	18,500	22,000	24,300	119	1.20	1.69	141
2	1,500	4,120	3,800	275	0.20	3.46	1730
3	2,000	5,340	5,290	267	0.40	2.55	638
			Elliptical Cutouts				
3-in. No. 1	13,600	17,000	18,530	125	0.420	1.064	253
2	3,400	5,310	5,450	156	0.366	2.133	582
3	3,600	6,360	6,890	177	0.087	0.781	898
4	2,950	5,200	5,230	176	0.255	1.401	549
5	4,200	7,900	8,280	188	0.082	0.600	737
6	2,400	4,670	5,130	195	0.296	1.684	571
7	2,400	5,850	6,320	247	0.117	1.216	1039
6-in. No. 1	33,000	46,550	51,440	141	0.337	0.562	167
2	7,000	10,650	10,240	152	0.280	1.800	643
3	6,900	11,880	11,160	172	0.095	0.701	737
4	7,500	12,290	11,770	164	0.315	2.200	698
5	7,800	15,230	17,790	195	0.079	0.400	506
6	4,650	10,310	10,310	222	0.255	1.350	526
7	4,600	12,490	12,410	272	0.112	1.300	1161
			Diamond Cutouts				
3-in. No. 7-D-1	4,000	7,700	7,640	193	0.110	0.835	759
7-D-2	4,200	8,260	9,760	229	0.100	0.930	930
6-in. No. 7-D-1	12,800	23,120	25,370	181	0.115	0.651	566

beams appears in Figs. 15, 16, 17, and 18. The beam dimensions, the dial gage locations, and the dial designation notation appear above each graph. Deflection bridges were used on the lower flange of the beam and the results appear in each graph. The deflection of the center of the span and of the quarter-points was also plotted.

The most interesting behavior pattern for 3-in. I-beam 2 appears in Fig. 15 for bridge T_1. The curvature of the lower flange increased at a progressively lower rate until just before failure when a more rapid increase occurred. All other deflections were linear functions of the load. The above behavior occurred for 3-in. I-beam 3, Fig. 16, except that no change occurred near failure. For 3-in. I-beam 5, the 6-in. bridge spanned part of two cutouts while the dial rested under an upright. In this instance the readings did not represent free flange curvatures, and the results coincided with the readings of the lower dials. All 3-in. beams retained a linear load-deflection characteristic to

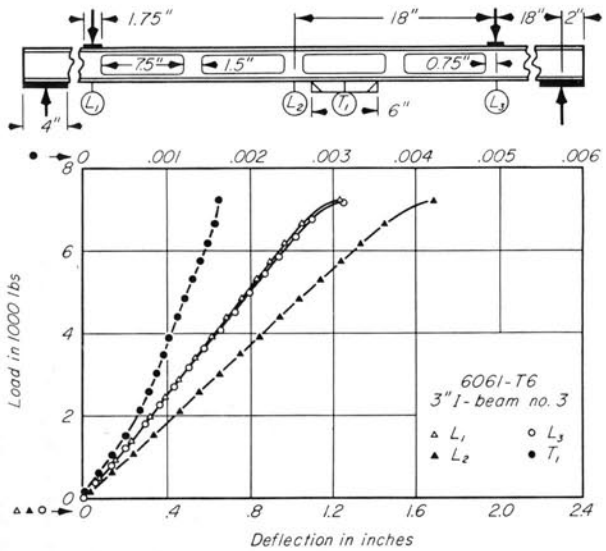

Fig. 16. Load-Deformation Behavior for 3-in. I-Beam No. 3, Rectangular Cutouts

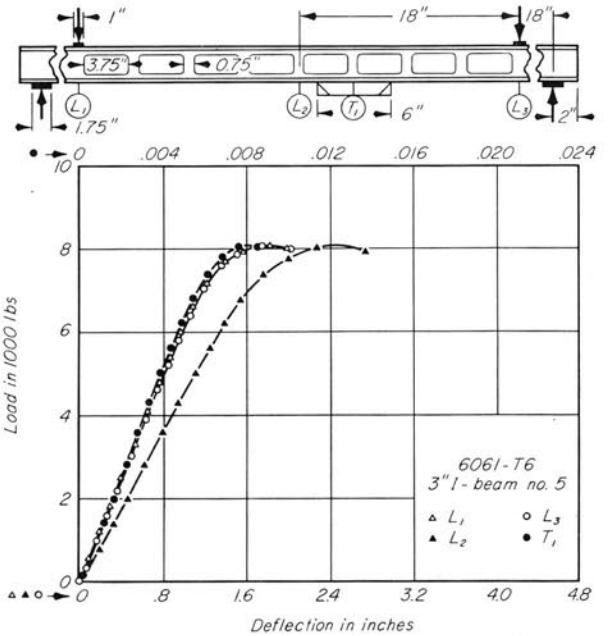

Fig. 17. Load-Deformation Behavior for 3-in. I-Beam No. 5, Rectangular Cutouts

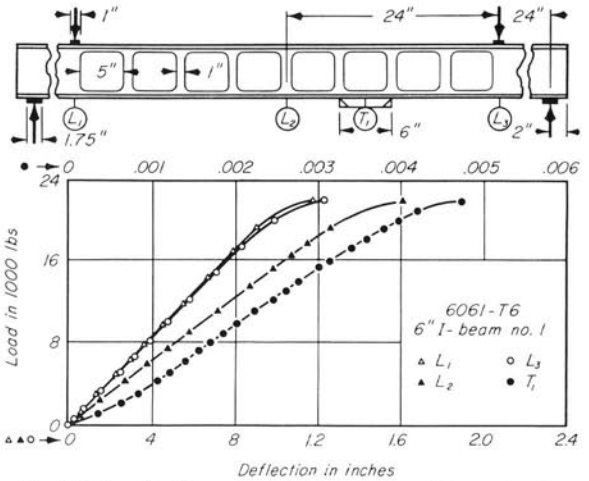

Fig. 18. Load-Deformation Behavior for 6-in. I-Beam No. 1, Rectangular Cutouts

approximately 85% of the maximum load. Six-in. I-beam 1 exhibited load-deflection behavior similar to that of 3-in. I-beam 5 with linear characteristics to approximately 85% of the maximum load. The data are summarized in Table 5.

10. Rectangular Cutouts — Center Loading

Two types of failure mechanisms developed with center loading for both the 3-in. and 6-in. beams. In the one type, Figs. 20 and 24, all but one of the fully-plastic hinges developed in the flange. Note that there is one more flange hinge

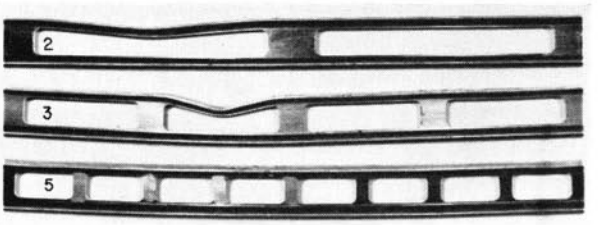

Fig. 19. Pure Bending Failures in 3-in. I-Beams, Rectangular Cutouts

for the beam in Fig. 20 than for the beam in Fig. 24. In the other type, Figs. 21 and 25, the major portion of the fully-plastic hinges developed in the web-section uprights between cutouts. The geometry of the first type is similar to the failure mechanism of a Vierendeel truss. These structures have been discussed extensively in the literature (see items 18 through 24 of the Bibliography).

The first failure mechanism developed when the fully-plastic strength of the web section between cutouts exceeded the fully-plastic strength of the flanges. The photograph of 3-in. I-beam 4B appears in Fig. 22, where it may be seen that a flange hinge developed at each quarter span in the lower flange for extremely large deflections. From the sequence of the development of the hinge mechanism in the upright and in the lower flange, it was apparent that the fully-plastic strength was only slightly greater for the upright than the lower web section. In the case of 6-in. I-beam 3, shown in Figs. 23

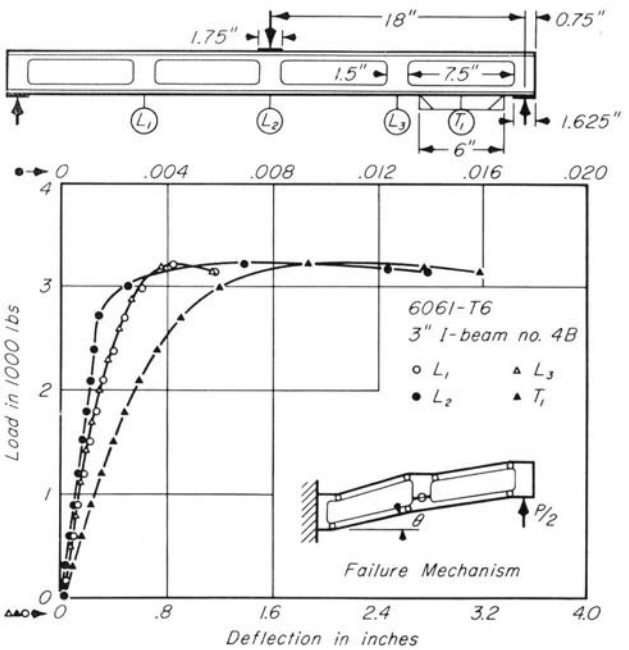

Fig. 20. Load Deformation Behavior for 3-in. I-Beam No. 4B, Rectangular Cutouts

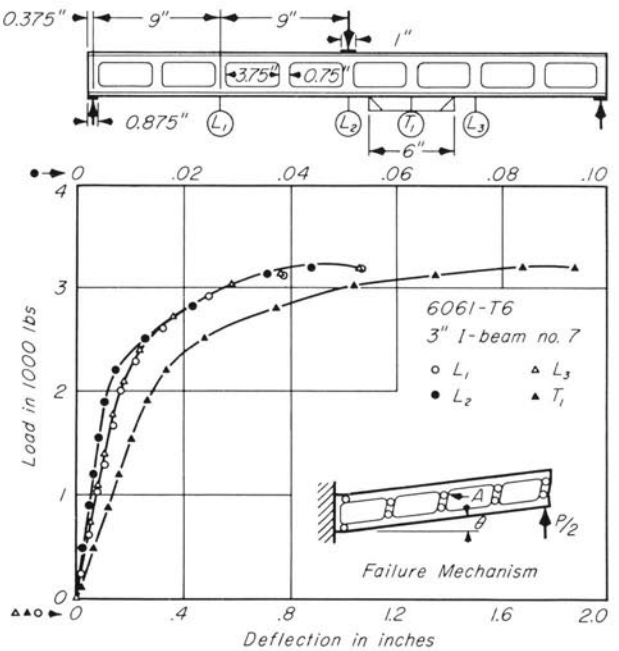

Fig. 21. Load Deformation Behavior for 3-in. I-Beam No. 7, Rectangular Cutouts

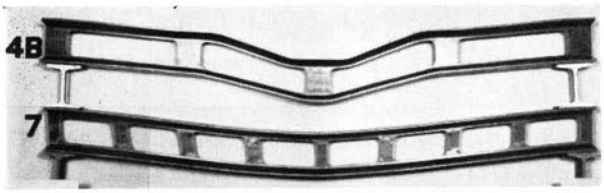

Fig. 22. Center Loading Failures in 3-in. I-Beams, Rectangular Cutouts

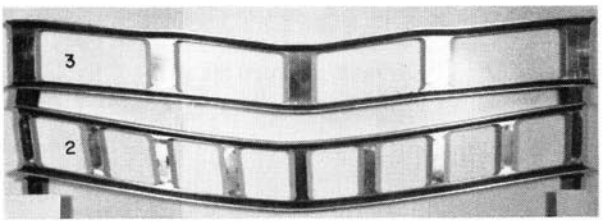

Fig. 23. Center Loading Failures in 6-in. I-Beams, Rectangular Cutouts

and 24, the hinge failure was confined almost entirely to the lower end of the upright between cutouts.

For both the 3-in. and 6-in. beams, the various panels deformed as parallelograms so that the end upright remained essentially vertical during deformation while the quarter-span upright rotated about its base. The bending moment varies linearly from zero at the outer end of the beam to a maximum at the center of the span while the vertical shear remains constant. Since the flange sections in the middle half of the beam were subjected to a greater moment, and since this value was greatest adjacent to the center upright, the flange sections failed by general yielding in that region first. General yielding followed in the flanges adjacent to the quarter-point and, last, in the end uprights.

The ultimate loads from theory reported in Table 5 were predicted on the basis of the development of six fully-plastic flange section hinges and one fully-plastic web-section hinge in each half of the beam, taking into account the attendant deformation geometry. The geometric considerations included an estimate of the point at which the fully-plastic hinge developed in the uprights. The location of the hinge varied. In some instances it occurred in the fillet at the end of the cutout. In other cases it occurred in the region away from the fillet. The Upper Bound Theorem was applied to obtain the estimated loads. The technique was similar to the outline in Section 4. In the present case, however, the procedure is far more complex, as it was necessary to try several failure mechanisms which would be possible with the geometry involved and determine the mechanism which led to the least load. For example, a mechanism which assumed that the truss deformed strictly as parallelograms, and thus had eight fully-plastic flange hinges with no web hinges, led to a higher load. Of all the failure mechanisms which were tried, the one presented resulted in the least load and agreed with the observed geometry.

The results in Table 5 for I-beams with rectangular cutouts show close agreement between the calculated load and the test load. The agreement is adequate to give confidence in the procedure when carefully used. A word of caution is appro-

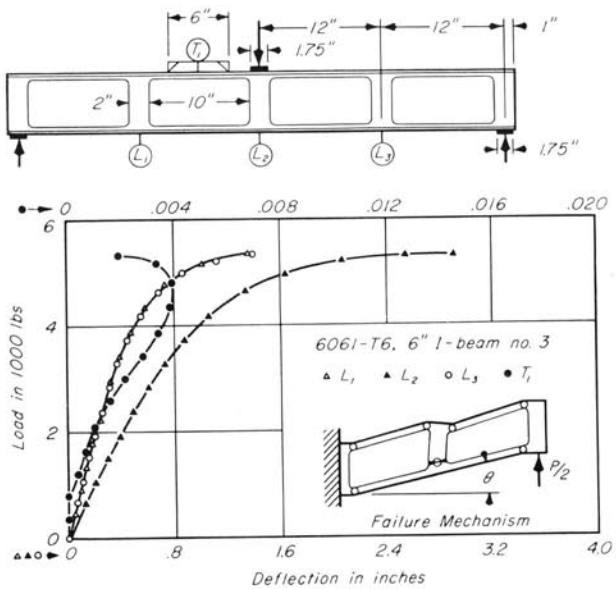

Fig. 24. Load-Deformation Behavior for 6-in. I-Beam No. 3, Rectangular Cutouts

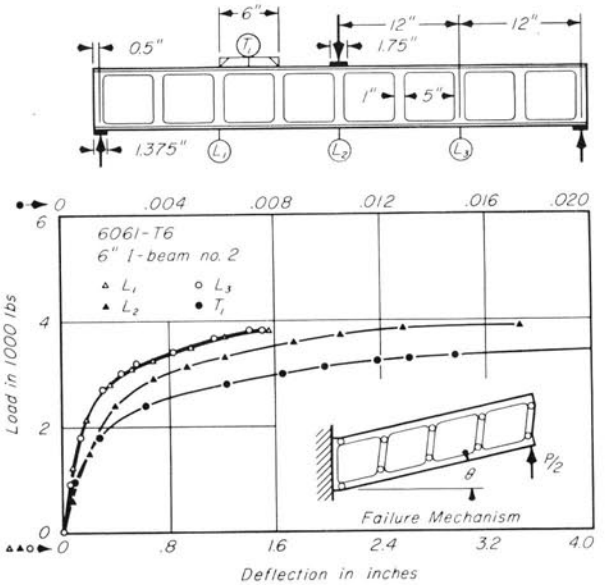

Fig. 25. Load-Deformation Behavior for 6-in. I-Beam No. 2, Rectangular Cutouts

priate here, however. Extreme care must be taken in evaluating all dimensions, and considerable insight into all possible geometric configurations is necessary to insure that the correct mechanism, the one giving the lowest load, has been visualized. Any other assumed mechanism could lead to an unsafe load. This is one weakness of the Upper Bound procedure. However this weakness is more than offset by saving in time and effort involved as compared with the application of the so called Lower Bound Theorem and procedures.[5]

The other failure mechanism mentioned at the beginning of this section, and displayed in Figs. 21 and 25, involved the development of fully-plastic hinges at the top and bottom of each web-section upright, accompanied by flange hinges adjacent to the center upright. Several other geometric configurations, including those which assumed the deformation of the beam in the shape of a curve, were analyzed to arrive at the mechanism resulting in the lowest load. The comparison of the test load and the calculated load for 3-in. I-beam 7 and for 6-in. I-beam 2 appears in Table 5.

The load-deflection behavior for 3-in. I-beams No. 4B and 7, as well as for the 6-in. I-beams 3 and 2, appear in Figs. 20, 21, 24, and 25, respectively. As in the case of pure bending, the dial gage locations and designations appear on the beam sketch above the graph. The deviation from the linear load-deflection relation occurred at 34.0, 48.5, 37.5, and 44.6% of the maximum load for 3-in. I-beams No. 4B and 7 and for 6-in. I-beams 3 and 2, respectively. The elastic deflections represented 13.0, 11.9, 5.8, and 15.6% of the ultimate-load deflection for the above beams.

The load-deflection diagrams show clearly that these beams had the ability to sustain large deflections at a nearly constant load near the ultimate load. The inverse curvature of the load deflection diagram for the 6-in. deflection bridge on 6-in. I-beam 3, Fig. 24, was due to the development of fully-plastic hinges, which resulted in the release of the positive curvature of the flange section to which the bridge was attached.

11. Elliptical Cutouts — Pure Bending

The pure bending test specimens with elliptical cutouts were only half as long as the equivalent specimens with rectangular cutouts. The cutout lengths and spacings were the same for both series of tests, however.

The 3-in. I-beam with elliptical cutouts failed by general yielding of the upper flange, Fig. 29, Beam 1. An unusual geometric pattern developed

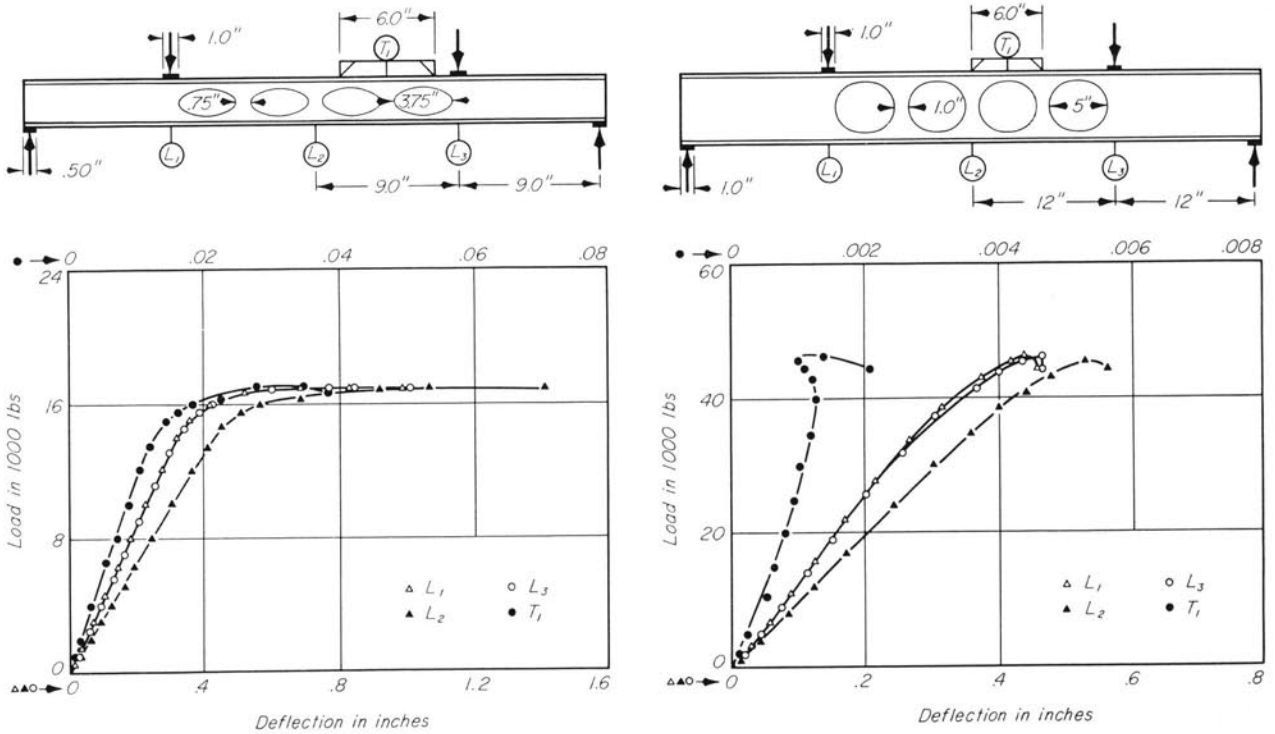

(a) 6061-T6, 3" I-beam no. 1

(b) 6061-T6, 6" I-beam no. 1

Fig. 26. Load-Deformation Behavior for 3-in. and 6-in. I-Beam No. 1, Elliptical Cutouts

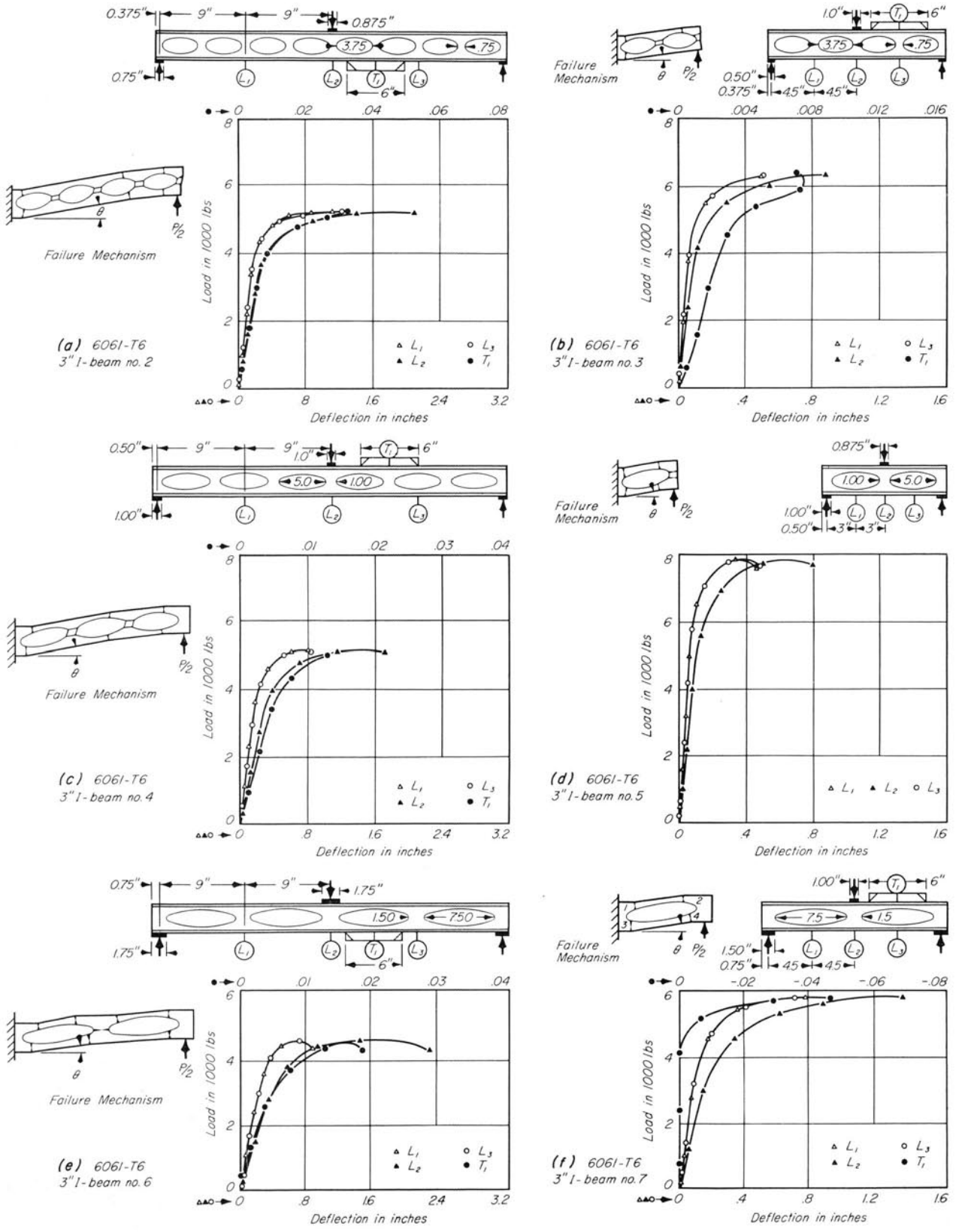

Fig. 27. Load-Deformation Behavior for 3-in. I-Beams with Elliptical Cutouts

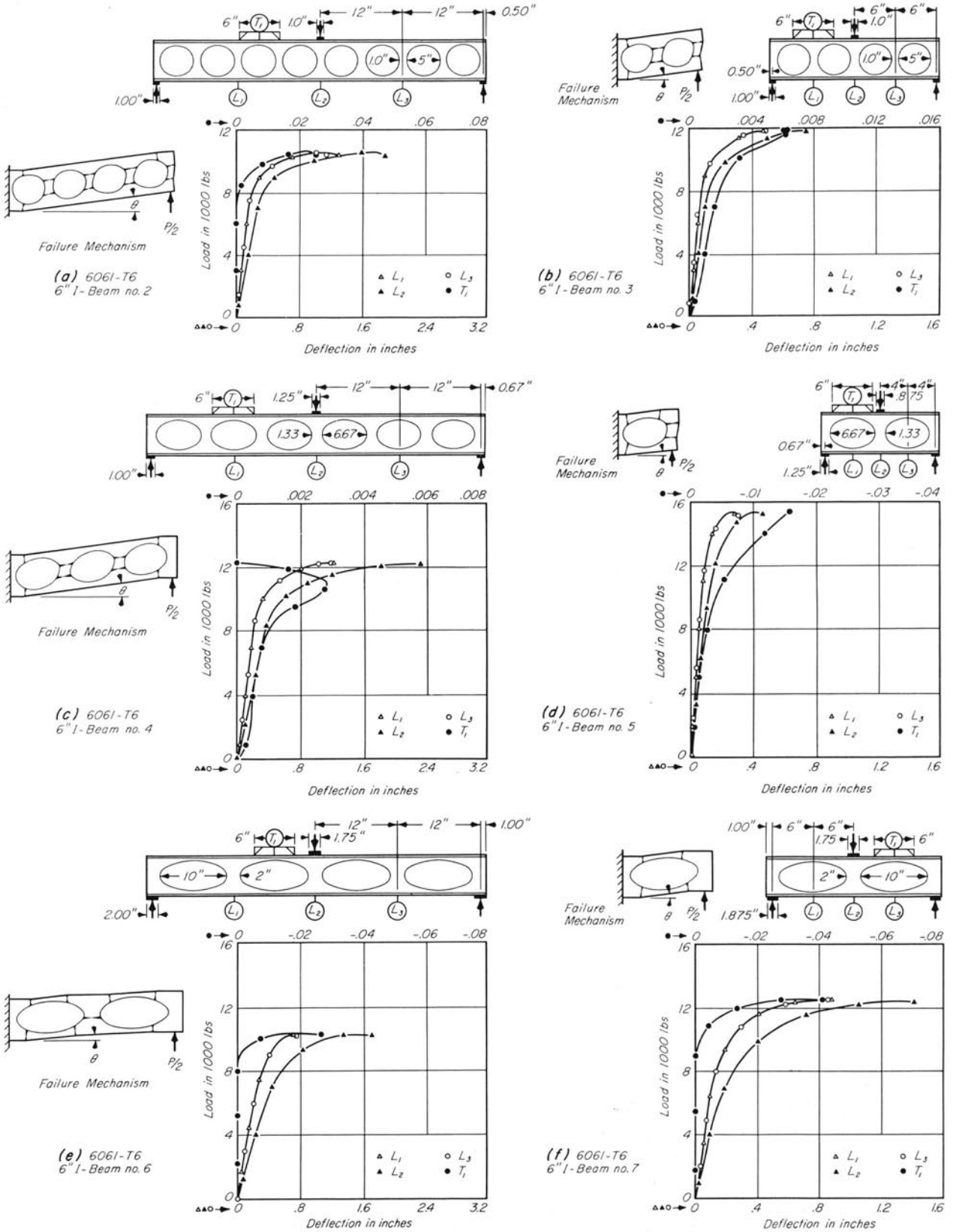

Fig. 28. Load-Deformation Behavior for 6-in. I-Beams with Elliptical Cutouts

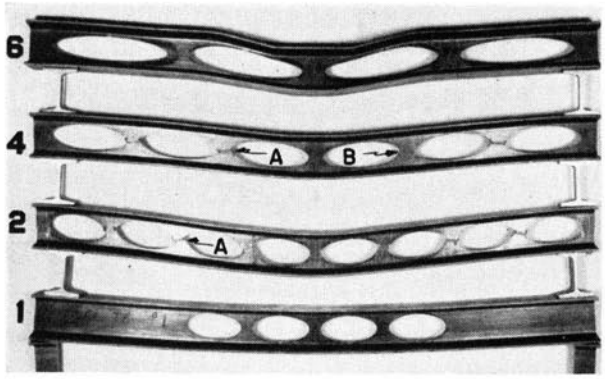

Fig. 29. 3-in I-Beam Failures: No. 1 in Pure Bending, Others with Center Loading

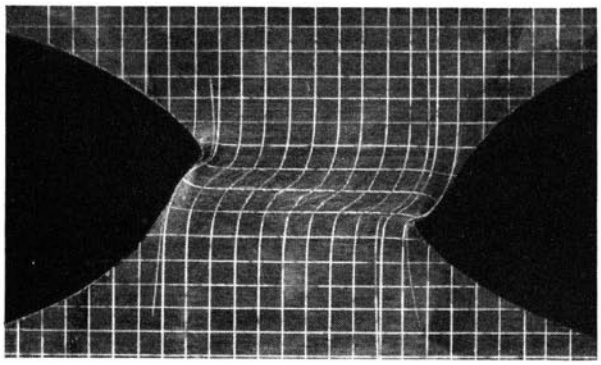

Fig. 30. Deformation of Upright "B" of 3-in. I-Beam No. 4

along the lower flange of this beam. Between the uprights, at the point where the flange section had the least depth, the flange was deflected upward 0.01 to 0.015 inches. Sections away from the minimum flange depth had neutral surfaces which were progressively farther from the outer surface of the I-beam. The axial forces acting through the elastic, partially inelastic, or fully-plastic neutral surfaces of the particular sections away from the minimum section, were not collinear. Therefore, the weaker sections tended to deflect upward in order to allow the forces, which acted through the neutral surfaces, to become collinear.

Local buckling of the solid web section above the end loading pads for the 6-in. I-beam had to be inhibited by clamping steel plates on the sides of the web-section. These plates extended 6-in. from the end of the beam. The 6-in. I-beam failed by buckling of the web section under the upper left loading block, Fig. 32, Beam 1. This failure was followed by local bending of the upper flange in the region just to the right of the buckling failure. Because of the nature of the cross-section in this region, solid web-section material extending to the left and the elliptical shape to the right, it was not practical to develop an expression for the theoretical failure load. Different widths of the upper loading pad might have altered the failure of these I-beams. However, the pad widths and positions were maintained constant for both types of loading to avoid introducing another variable.

The load-deformation behavior for the 3-in. and 6-in. I-beams in pure bending appear in Fig. 26, along with diagrams indicating the designation and location of each dial gage. Since 3-in. I-beam 1 failed by general yielding, there were no unusual phenomena to be discussed in this case. The load remained constant over a rather large deflection range. The effect of the web-section buckling that occurred below the upper left loading pad at the ultimate load for 6-in. I-beam 1 is seen in Fig. 26b, where the load dropped abruptly.

The unusual deflection behavior measured by the 6-in. bridge was due to the tendency of the upper flange sections to arch upward over a cutout in the middle of the span. This arching effect was produced by the same phenomenon which caused the bending away from the outer surface of the beam on the tension side of the member discussed earlier. In this case, however, the eccentricity of the neutral surface of successive sections promoted arching away from the common neutral surface line due to the compressive forces. The bridge first registered an increase in curvature, followed by a decrease in curvature as the arching effect became prominent. However, the deflection increased again when the local failure of the flange near the left upper load permitted a release of the compressive strains in the upper flange of the beam.

The predicted failure loads, listed in Table 5, for the above beams were obtained by assuming that a fully-plastic hinge was developed at the minimum section in a cutout adjacent to a quarter-point load. The hinge consisted of the upper flange which was in compression and the lower flange which was in tension. Moments developed within the individual flanges were assumed to be negligible in these calculations. The 3-in. and 6-in. I-beams carried 104 and 106% of the load carried by the equivalent I-beams with rectangular web-section cutouts discussed earlier.

12. Elliptical Cutouts — Center Loading

The failure mechanisms which developed in the inelastic load range are shown in Figs. 27a through 28f. Two types of failure mechanisms developed: shear failures represented by the web-section paral-

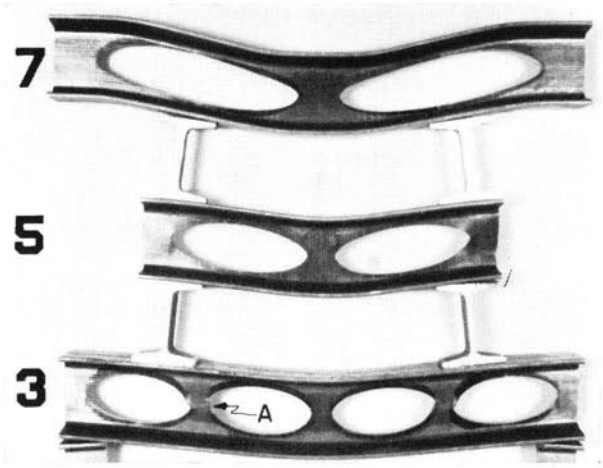

Fig. 31. Center Loading Failures of 3-in. I-Beams

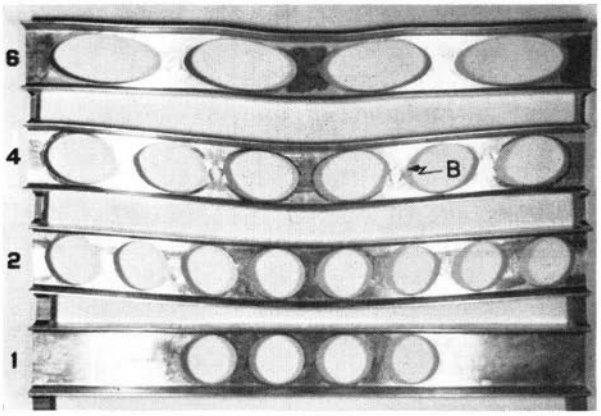

Fig. 32. 6-in. I-Beam Failures: No. 1 in Pure Bending, Others with Center Loading

lelograms and bending moment failures represented by the yield wedges which formed fully-plastic hinges as in the flange and in the end web section (Fig. 27a). In addition, buckling failures developed in the uprights for 3-in. I-beams 3 and 5, and for 6-in. I-beams 2, 3, 4, and 5. A view of the buckling failure for 3-in. I-beam 5 appears in Fig. 14. This beam sustained the highest load for center loaded 3-in. I-beams with elliptical cutouts.

Of all of the beams tested with elliptical cutouts, only 3-in. I-beams 2, 3, and 4 exhibited shear failures in the web section, see Fig. 27a, b, and c. These failures resulted in complete separation of the uprights indicated by A in Figs. 29 and 31. The shear failures were sudden fractures. However, the release of the resisting shear force did not result in any appreciable release in the load carried by the beam. An enlarged view of upright B from Fig. 29 appears in Fig. 30; grid spacing is 0.1 in.

The load-deflection relations, Figs. 27a through 28f, will now be considered. The scales for load and for deflection vary from one graph to another. The scales used for the 6-in. span deflection bridge appear across the top of the load-deflection curves. The scale factors were selected to give a suitable horizontal scale in this case. Although the elliptical cutouts in Fig. 28a and b appear to be circles, they have a length of 5 in. and a height of 4.5 in.

All of the tests reported here had companion specimens which were loaded in the same manner but which had a shorter span length and a correspondingly higher ratio of shear to bending moment. The even numbers designated the long span specimens in every case. The companion tests were 2-3, 4-5, and 6-7 for the 3-in. and 6-in. I-beams. The span of specimen 5 is one-third the span of the longer companion specimen. The span ratio was 2 to 1 for the beams 2-3 and 6-7. This should be

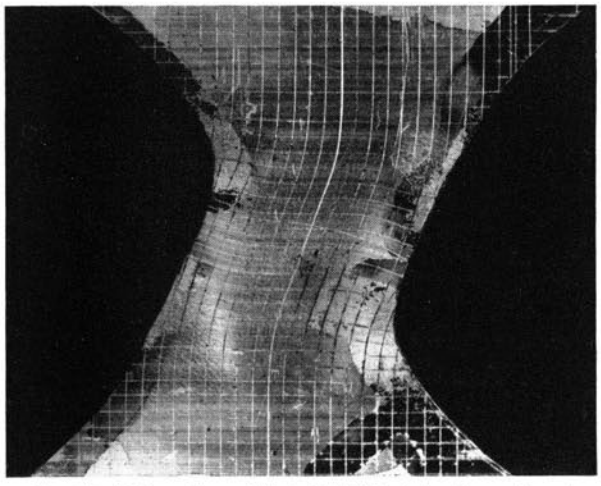

Fig. 33. Deformation of Upright "B" in 6-in. I-Beam No. 4

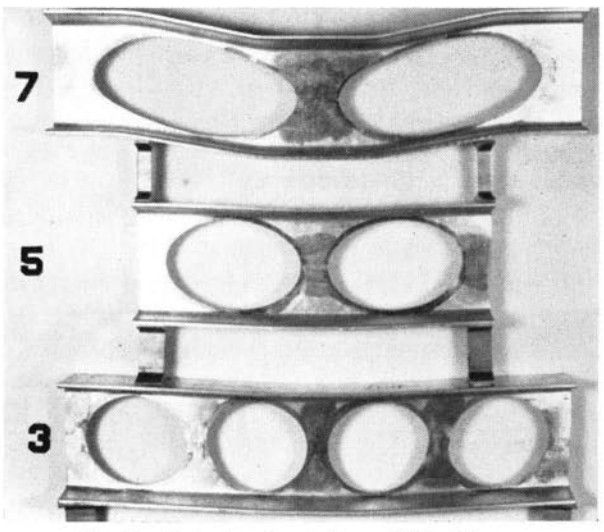

Fig. 34. Center Loading Failures of 6-in. I-Beams

remembered when comparing the values for midpoint deflection from Table 5.

Some insight into the nature of the failure, whether by formation of the plastic hinges or by buckling of an upright section under a loading point, can be gained by observing the slope of the load-deflection curve just prior to the ultimate load. For all long spans the slope of the curve changes very gradually, indicating the progressive development of inelastic hinges and inelastic shear regions. It is evident for both 3-in. and 6-in. I-beam 5 that the load-deflection curve rises very rapidly up to the point of failure. This behavior was due to buckling of the web-section material.

The behavior of the load-deflection reading for the 6-in. I-beam 4 deflection-bridge, T_1, may be interpreted as follows: The upper flange first deformed downward as the beam deflected, then, as hinges began to develop in the uprights between the cutouts, the section of the beam in this region started to relax, and decrease in curvature. More precisely, the three points constituting the ends of the bridge and the center of the bridge were again on a straight line. While this condition could have occurred without having a straight section between these points, the section was essentially straight. This reverse in curvature can be seen in Fig. 28c. In the same way, the impending failure of the web section for 3-in. I-beam 3, Fig. 27b, can be seen from the reversal of the load-deflection curve for the 6-in. deflection bridge.

The column heading *Load, Ultimate Divided by Proportional Limit* in Table 5, represents the ratio of the ultimate load-carrying capacity to the elastic load-carrying capacity in percent. When presented in this manner, these figures represent the reserve load-carrying capacity up to the point of complete structural failure. In all cases the shorter-span specimens had a greater reserve load-carrying capacity than their respective longer-span companion specimens.

Of the various geometric configurations of the long beams with elliptical cutouts, 3-in. I-beam 2 and 6-in. I-beam 4 exhibited the greatest load-carrying capacities. These beams also experienced the greatest ultimate-load deflections (see Table 5).

The values of the ultimate load from the theory for elliptical cutouts, reported in Table 5 for 3-in. and 6-in. I-beam 2 through 7, were obtained using the Upper Bound Theorem as discussed in Section 4. The mechanism analysis assumed the energy to be dissipated either in fully-plastic hinges or in shear deformation regions. Careful study of Fig. 33, which represents upright B of 6-in. I-beam 4 in Fig. 32, reveals that there is a band of distorted material approximately five grid lines in width, indicating a nearly pure shear failure. The grid lines in the regions on either side of this band form nearly true rectangles while the lines inside the band form parallelograms. These two regions indicated an interaction effect between shear and moment. A calculation of the energy dissipated in the upright, however, revealed that there was a negligible difference in computed values obtained by assuming the energy to be distributed in shear and in bending and by assuming that two fully-plastic hinges existed, one being in the upper and the other in the lower portion of the upright. The failure mechanism appears in Fig. 28c.

All 3-in. I-beams 2 through 7 developed hinge mechanisms. The shear mechanism was used in addition to the hinge mechanism for 3-in. I-beams 2, 3, and 4. The shear deformation regions which developed in the upright between loading points predominated over the tendency to develop hinges in these regions. All 6-in. I-beams 2 through 7 developed hinge mechanisms only. The middle upright under the center load developed no mechanism but the end upright over the end load developed hinge mechanisms for 3-in. and 6-in. I-beams 2, 3, and 5.

The application of the mechanism analysis using the Upper Bound Theorem for the I-beams with elliptical web-section cutouts was extremely complex in terms of the computations involved. The complexity was caused by the varying width of web section in the uprights and particularly by the varying depth of flanges and web sections which constituted the sections participating in the development of fully-plastic hinges.

The flange above or below a cutout was a "T" section. The depth of the "T" section changed as the hinge was located at various points along the length of the ellipse. This factor was also discussed in Section 4.

The values of ultimate load from theory appear in Table 5. The percent deviations from the test load, using the test load as a reference, for 3-in. I-beams 2 through 7 were +2.6, +8.3, +0.58, +4.8, +9.8, and +8.0%. The percent deviations for 6-in. I-beams 2 through 7 were −3.9, −6.5, −4.2, +16.8, 0, and −0.64%. No interaction effects were considered, and these effects may account for the consistent deviation on the high side

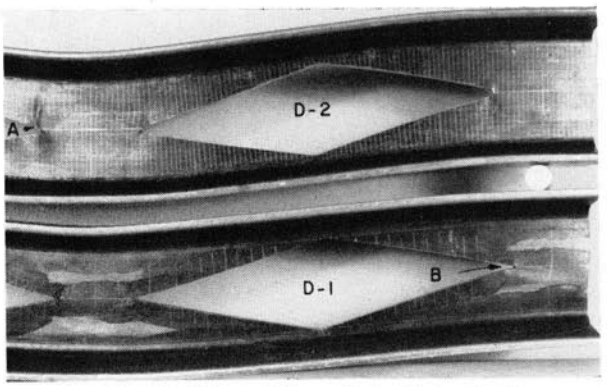

Fig. 35. 3-in. I-Beam Failures Under Center Loading, Diamond-Shape Cutout

for the 3-in. I-beams and on the low side for the 6-in. I-beams. There were insufficient interaction data to draw any conclusions concerning this effect in either set of tests. The one exception is 6-in. I-beam 5, which exhibited pronounced buckling of one of the end uprights.

13. Diamond-Shape Cutouts — Center Loading

This program was initiated with the knowledge of the ILLIAC solutions which predicted the diamond-shape web-section cutouts to be the strongest in terms of load-carrying capacity per pound of beam. The ILLIAC solutions applied only to 3-in. and 6-in. I-beams with the same dimensions as beam type 7 of the elliptical-cutout test program. (Thus, the beam designated as 7-D-1 indicated beam type 7, diamond-shape web section cutouts, specimen 1.)

A pilot test of 3-in. I-beam 7-D-1 was conducted using a diamond-shape cutout with very small end radii. The strength of the beam was so great in bending, however, that a shear failure mechanism developed at the right end, see B in Fig. 35. The failure line extended from the end of the cutout to a point at the extreme right, approximately 0.5 inch below the horizontal center line.

A simplified analysis of the above beam failure was obtained by passing a vertical section through the beam at the center of the right cutout. Application of the moment equation, with the assumption that the flange moments could be neglected and that a compressive force, C, acted at the upper flange, led to the following:

$$C\,(h - 2y) = \left(a + \frac{q}{2}\right)\frac{P}{2} \qquad (27)$$

The terms in Eq. 27 are identified in Figs. 1 and 2. Equating the compressive force to the shear force at B in Fig. 35, one obtains:

$$P = \frac{4tq\,(h - 2y)\,\tau}{2a + q} \qquad (28)$$

where τ is the average shear strength and is reported[8] as 25,000 psi. Equation 28 yields $P =$ 7,640 lb as compared with a failure load of $P = 7{,}700$ lb.

Because of the mode of failure of this beam and the excellent agreement with Eq. 28, the mechanism analysis was not applied. However, a second test with 3-in. I-beam 7-D-2 was conducted with the end throat length increased one-third, from 1.5 to 2.0 inches. The increase in the end throat length resulted in the development of a true four-link hinge failure mechanism as shown in Fig. 2b. The fully-plastic load was not realized, however, since a tear developed in the web section just above the arrow at A in Fig. 35. This accounted for the sudden drop following the maximum load as shown in Fig. 36b. The increase in each throat area was achieved by maintaining the same distance between loading points, retaining the same shape of cutout, drilling a hole at either end of the diamond and adding 0.25 in. on each end of the I-beam. The hole had a 0.0781-in. radius which left 0.25 in. of solid material inside the point $u = a = 3.75$ in. A radius of 0.0625-in. was used at $v = b = 0.875$ in. This preserved the shape of the diamond, moment arms, etc. The decrease in the area of the cutout resulting from the end radii was 0.55%.

A similar modification was applied in turn to 6-in. I-beam 7-D-1 using a 0.25 in. radius at either end of the diamond. A radius of 0.0625-in. was used at $v = b = 2.25$ in. The decrease in the area of the cutout resulting from the end radii was 0.60% for this beam. This modification was justified since the beam carried an ultimate load of 23,120 lb; applying Eq. 28 to this beam (without increasing the throat area), and using the reported[8] value of shear strength $\tau = 24{,}000$ psi, yields a load $P = 20{,}500$ lb. Thus, this beam would have failed by shear if the end throat area had not been increased.

The load-deflection behavior for the three I-beams with diamond-shape cutouts appears in Fig. 36. A photograph of the deformation behavior for 6-in. I-beam 7-D-1 is shown in Fig. 37. The 0.1 in. grid lines depict the deformation behavior. The results of the tests with diamond-shape cutouts appear at the bottom of Table 5.

Table 6

Comparison of Results for Constant Cutout Length

Cutout Shape	Solid	Diamond	Ellipse	($\alpha=\beta=9$)	Rectangle
3-IN. I-BEAM TYPE NO. 7					
Proportional Limit Load, lb	14,000	4,200	2,400	.....	.....
Ultimate Load, P, lb — Test	18,150	8,260	5,850	.....	.....
Ultimate Load, P, lb — Calculator	22,600	9,760	6,320	.....	3,860
Ultimate Load, P, lb — ILLIAC	.....	9,820	6,470	3,910	.....
(Ultimate Test Load / Proportional Limit Load), %	130	229	247	.....	.....
Weight Removed, %	0	7.40	11.68	14.63	14.69
Weight of Beam, W, lb	2.940	2.723	2.597	2.510	2.508
Test Load Capacity, (P/W)	6,170	3,030	2,250	.....	1,540*
ILLIAC Load Capacity, (P/W)	.....	3,610	2,490	1,560	.....
((P/W) Cutout / (P/W) Solid), %	100	49.1	36.5	25.3†	25.0*
Mid-Point Deflection, in., Prop. Limit Load	0.108	0.100	0.117	.....	.....
Mid-Point Deflection, in., Ultimate Load	0.231	0.930	1.216	.....	.....
(Ultimate Load Deflection / Prop. Limit Load Deflection), %	214	930	1,039	.....	.....
6-IN. I-BEAM TYPE NO. 7					
Proportional Limit Load, lb	38,000	12,800	4,600	.....	.....
Ultimate Load, P, lb — Test	44,820	23,120	12,490	.....	.....
Ultimate Load, P, lb — Calculator	69,800	25,370	12,410	.....	5,840
Ultimate Load, P, lb — ILLIAC	.....	29,340	13,200	6,420	.....
(Ultimate Test Load / Proportional Limit Load), %	118	181	272	.....	.....
Weight Removed, %	0	11.72	18.52	23.18	23.48
Weight of Beam, W, lb	8.60	7.592	7.007	6.607	6.581
Test Load Capacity, (P/W)	5,210	3,050	1,780	.....	887*
ILLIAC Load Capacity, (P/W)	.....	3,870	1,880	970	.....
((P/W) Cutout / (P/W) Solid), %	100	58.5	34.2	18.6†	17.0*
Mid-Point Deflection, in., Prop. Limit Load	0.108	0.115	0.112	.....	.....
Mid-Point Deflection, in., Ultimate Load	0.144	0.651	1.300	.....	.....
(Ultimate Load Deflection / Prop. Limit Load Deflection), %	133	566	1,161	.....	.....

* Load obtained using desk calculator.
† Load obtained using ILLIAC.

A comparison of the two columns of ultimate strength in Table 5 shows that the agreement between test load and calculated load is less favorable for 3-in. I-beam 7-D-2 and 6-in. I-beam 7-D-1 than for the beams with rectangular or elliptical cutouts. The failure load calculation for 6-in. I-beam 7-D-1 appears in Table 4. The constants in Table 4 were those which applied to 6-in. I-beam 7-D-1 and are not the same as the nominal values of Eqs. 1, 2, and 3 of Section 4. Deviations of the calculated loads from the test loads were caused by an unpredicted deflection of the web section under the center load and by neglecting elastic core effects near the neutral surfaces of the hinges. The load was first calculated using Eq. 20. The second value of the load was determined using the true distance through which the load $P/2$ moved. These two values of load appear at the bottom of Table 4. The ultimate loads for 3-in. I-beam 7-D-2 and 6-in. I-beam 7-D-1 were calculated using the true hinge locations as measured on the beams and the measured beam dimensions.

The assumption that hinge No. 1 in the lower left corner of Fig. 2b remained at a fixed distance above the lower surface of the beam was not justified in the case of the 6-in. I-beams. Actually, the beam curved along the lower surface and an upward deflection of 0.04 in. existed at hinge No. 1. This changed the distance through which the load moved from 0.51 to 0.55 in. The greater movement increased the work done by the load. Therefore, the value of P obtained by equating the external work with the internal work was reduced proportionately. The value of P reported in Table 5 was obtained using the measured displacement of 6-in. I-beam 7-D-1. For 3-in. I-beam 7-D-2 the above corrections were unnecessary.

Web-section buckling in 6-in. I-beam 7-D-1 caused a reduction in the test load below that predicted by the calculations. The web section immediately below the center of the upper loading pad experienced local buckling at a point 1.5 in. below the upper surface of the I-beam. The affected region was about 1.25 in. wide and 1.0 in. high. The above factors contribute to the test load of 23,120 lb compared to the predicted load of 25,370 lb.

Two solid web-section I-beams, 3-in. No. 7-S and 6-in. No. 7-S, failed by buckling under the upper loading pad accompanied by general yielding of the upper flange. The same span and loading pad width were used in each case as for the corresponding I-beam with the diamond-shape cutout.

The calculated failure loads shown in Table 6 for the solid web-section I-beams were obtained by assuming the development of fully-plastic hinges. Since the failure was by general yielding of the upper flange, accompanied by buckling of the web section below the upper loading pad, the calculated

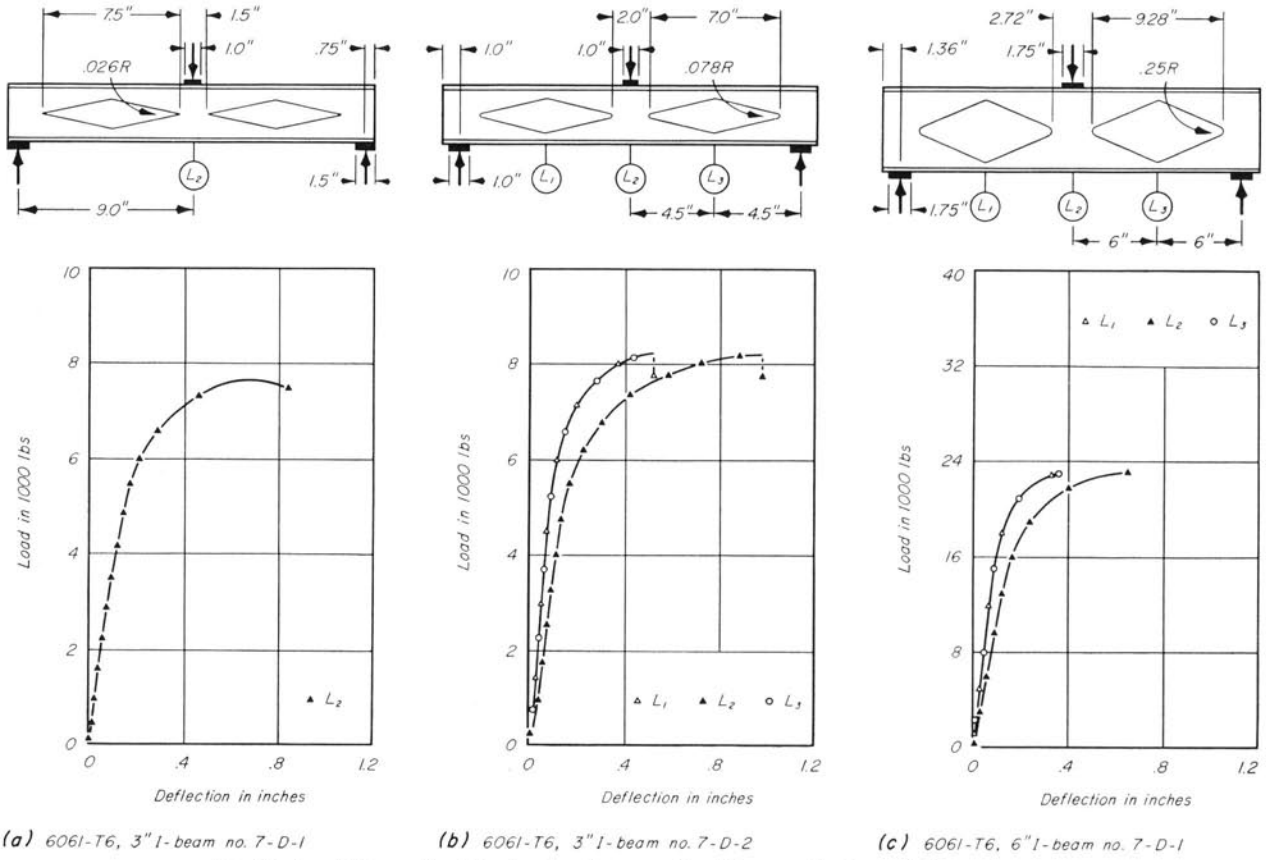

(a) 6061-T6, 3" I-beam no. 7-D-1 (b) 6061-T6, 3" I-beam no. 7-D-2 (c) 6061-T6, 6" I-beam no. 7-D-1

Fig. 36. Load-Deformation Behavior for 3-in. and 6-in. I-Beams with Diamond-Shape Cutouts

loads exceeded the measured loads. The deviation was greater for the 6-in. I-beam since the buckling effect was more pronounced.

14. Comparison of Results for Constant Cutout Length

The data presented in Table 6 are intended to show a comparison of results for beams of Type 7. Most of the values also appear in Table 5. It should be noted that, for both the 3-in. and 6-in. beams, the solid section is the strongest and has the least deflection and lowest ratio of ultimate-load deflection to proportional-limit-load deflection. The ratio of test load capacity, $(P/W)_{\text{cutout}}$ divided by $(P/W)_{\text{solid}}$, shows the marked reduction in strength of the cutout specimen, dropping to 25.0 and 17.0% for the 3-in. and 6-in. I-beams with rectangular cutouts. For elliptical cutouts the values were 36.5 and 34.2%, while they were 49.1 and 58.5% for the diamond-shape cutouts for the 3-in. and 6-in. I-beams, respectively.

The comparison of the actual ultimate load with the predicted ultimate load obtained by the calculator for 3-in. I-beam 7-D-2 showed that the deviation from the test load was +18.2% due to the tearing of the metal as discussed earlier. The same comparison for 6-in I-beam 7-D-1 showed a +9.73% deviation.

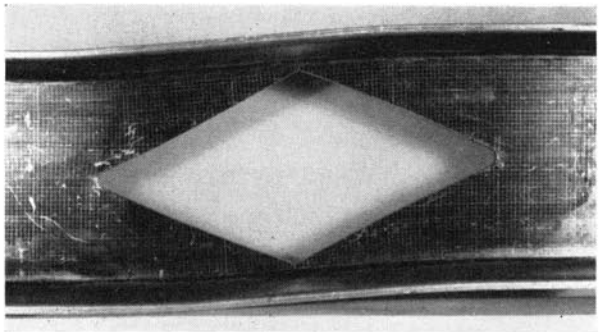

Fig. 37. Center Loading Failure of 6-in. I-Beam with Diamond-Shaped Cutout

V. CORRELATION OF ILLIAC RESULTS WITH TEST RESULTS

For 6-in. I-beam 7-D-1, the discrepancy between the ILLIAC value of load and the load obtained in Table 4 was due largely to the difference in the location of the hinges as determined with the ILLIAC and as measured on the beam. A comparison of the ILLIAC results, using the Upper Bound Theorem to locate the hinges at a point leading to a minimum load, with the measured values follow:

	u_1	u_2	u_3	u_4
ILLIAC	2.56	3.52	2.48	1.78
Measured	3.00	3.34	2.05	3.18
Deviation, %	−14.7	+5.4	+21.0	−44.0

The measured values were located by means of a 2-in. span dial bridge. The hinge was assumed to exist at the point where the curvature was maximum. Substitution of the measured hinge values into the ILLIAC program yielded $P = 30{,}280$ lb as compared with $P = 29{,}340$ lb for the minimized hinge location, indicating that the theoretical hinge locations lead to a lower minimum. This indicates that other factors, such as buckling of the web, influence the failure and location of the hinges of the test beam. The greatest deviation in hinge location occurs at u_4 because of the general yielding in this region.

For 3-in. I-beam 7-D-2, the hinge locations and the deviations were:

	u_1	u_2	u_3	u_4
ILLIAC	3.68	3.68	3.16	2.56
Measured	3.34	3.34	2.18	3.40
Deviation, %	+10.2	+10.2	+45.0	−24.7

Again, substitution of the measured hinge values into the ILLIAC program yielded $P = 10{,}050$ lb as compared with 9,820 lb for the minimized hinge locations.

The hinge locations of the elliptical cutout and the deviations for the 3-in. I-beam were:

	u_1	u_2	u_3	u_4
ILLIAC	2.90	3.00	2.72	2.58
Measured	3.10	3.18	2.40	2.70
Deviation, %	−6.5	−5.7	+13.3	−4.4

The hinge locations of the elliptical cutout and the deviations for the 6-in. I-beam were:

	u_1	u_2	u_3	u_4
ILLIAC	3.00	3.22	2.96	2.74
Measured	3.35	3.65	2.78	3.23
Deviation, %	−10.4	−11.8	+6.5	−15.2

These values are in substantially better agreement than those obtained for the diamond-shape cutouts primarily because there was no buckling of the web-section to shift the location of the fully-plastic region.

Another evaluation of the strength of the diamond-shape cutout was made by comparing its strength with that of the elliptical and rectangular cutouts of equal areas. The following dimensions give equal areas for each type cutout. With $b = 0.875$ in., for the 3-in. I-beam $a_D = 3.75$ in., $a_E = 2.385$ in., and $a_R = 1.875$ in. With $b = 2.25$ in. for the 6-in. I-beam, $a_D = 5.00$ in., $a_E = 3.18$ in., and $a_R = 2.50$ in. The values of (P/W) for a_E were computed using the ILLIAC while the values for a_R were obtained with the desk calculator. These values of (P/W) for the 3-in. I-beam were $(P/W)_D = 9{,}820$, $(P/W)_E = 10{,}170$, and $(P/W)_R = 8{,}530$ while those for the 6-in. I-beam were $(P/W)_D = 29{,}340$, $(P/W)_E = 20{,}700$, and $(P/W)_R = 12{,}690$. The experimental values were $(P/W)_D = 8{,}260$ and 23,120 for the 3-in. and 6-in. I-beams as reported in Table 4. Experimental results were not obtained for the elliptical and rectangular cutouts described above. The experimental data available in references 1 and 2, however, lead to the conclusion that the experimental values would be approximately $(P/W)_E = 9{,}000$ and 19,600 for 3-in. and 6-in. I-beams, respectively. The experimental values of $(P/W)_R$ would be expected to remain nearly equal to the predicted values.

The above comparisons show that for 3-in. I-beams with these particular geometries, the strength variation between the three shapes of cutouts is small for equal cutout areas. For the 6-in. I-beams, the diamond results in the strongest beam for equal cutout areas.

The greater sensitivity of the 6-in. I-beam to the cutout shape, for constant area removed, may be due in part to the difference in distribution of the total cross-sectional area between the flange and the web. For the 3-in. I-beam, 82.3% of the area is contained in the flanges as compared to 70.8% in the flanges of the 6-in. I-beam.

VI. SUMMARY AND CONCLUSIONS

15. Summary of Results

The most important outcome of the series of tests on beams with rectangular cutouts was the determination of the elastic and inelastic load-deflection behavior. The tests also served to verify the accuracy of the Upper Bound Theorem for predicting the fully-plastic load-carrying capacity of 6061-T6 aluminum alloy I-beams. The theory does not apply where the beam failure results from buckling or tearing of the upright. Thus, if there is any uncertainty as to the mode of failure, it is mandatory that tests shall be conducted rather than relying on the Upper Bound Theorem.

The results of the tests with elliptical web-section cutouts helped establish a better understanding of the failure mechanisms which might be expected with a more general cutout contour.

A comparison between the load-carrying capacity of the I-beams with elliptical web-section cutouts and that of I-beams with rectangular web-section cutouts showed very little advantage was to be gained for pure moment loading, but under certain types of loading the strength improved greatly for elliptical cutouts as compared with rectangular cutouts.

The third phase of the project involved the use of the above information in developing a suitable set of mathematical relations to permit programming on the ILLIAC digital computer. The results of the analysis for a simple beam with elliptic-type cutouts predicted the diamond-shape cutouts to be the strongest for center loading when the same length of cutout was used for all I-beams. The rectangular, elliptical, and diamond-shape cutouts are all special cases of the elliptic-type cutout.

A subsequent analysis was conducted for constant web-section area removed from each beam. This analysis showed the diamond-shape cutout to be the strongest shape for the 6-in. I-beams, and indicated that for 3-in. I-beams the shape of the cutout was not a major factor affecting the strength. For the 3-in. I-beams the elliptical cutout shape yielded the most favorable result among the rectangle, the ellipse, and the diamond.

The analytical and experimental work on diamond-shape cutouts did not include multiple cutouts in either end of the I-beam. Such data would be useful in extending the knowledge of inelastic behavior beyond this point. Some work of this nature has been reported for welded steel I-beams,[11] where hexagonal cutouts were used.

As stated in Section 2, the report attempts to answer "What shape cutout results in the least reduction in fully-plastic load-carrying capacity per pound of beam weight?" It has not been fully answered here as much more information is needed for a complete answer. The reader should keep the limitations in mind when reviewing the conclusions.

16. Conclusions

The conclusions apply to one specific material, aluminum alloy 6061-T6, which has a relatively flat-topped stress-strain diagram and high ductility. The conclusions cannot be extended to less ductile aluminum alloys, which may be much more sensitive to stress concentrations, without verification. Aluminum alloy 2014-T6, for example, proved to have insufficient ductility to permit good agreement for one beam configuration.[6]

A. When subjected to center loading, an aluminum alloy 6061-T6 I-beam with a single, diamond-shape, web-section cutout (with end radii) in either half of the beam exhibits the highest load-carrying capacity, as compared to the solid web-section I-beam, of any of the cutout configurations considered. The above cutouts were of equal length, neglecting the slight end radii correction for the diamond-shape cutout.

B. The ultimate load-carrying capacity of aluminum alloy 6061-T6 I-beams can be predicted within $\pm 11\%$ by using the Upper Bound Theorem and the mechanism method of analysis for cutout configurations which do not result in excessive stress concentrations or tearing of the metal before the fully-plastic load can be developed. The test results show two exceptions to the above statement. One is 6-in. 5 elliptical cutout; the other is 3-in. 7-D-2. In the case of the 6-in. beam, buckling

occurred in the web section, while tearing was observed in the 3-in. beam. Since the Upper Bound Theorem does not hold for failures of these types, the predicted load did not fall within 11% of the test load.

C. The deviation of the predicted load from the experimental load becomes larger as the transition is made from the rectangular to the diamond-shape cutout. This was due to the inability of the assumed deformation geometry to fit the true deformation behavior because of general yielding in the flange and buckling of the web section under the center load as the cutout approaches the diamond shape.

D. On the basis of equal area of cutout, with a single cutout in each half span, the elliptical cutout shape was stronger than the diamond-shape or the rectangular-shape cutout for the 3-in. I-beams. For the 6-in. I-beams the diamond-shape cutout was the strongest for equal cutout areas.

VII. REFERENCES

17. Material Cited

Arranged in order of citation.

1. Neal, B. G., *The Plastic Methods of Structural Analysis,* John Wiley & Sons, Inc., 1956.

2. Greenberg, H. J. and Prager, W., "Limit Design of Beams and Frames," *Transactions ASCE,* Vol. 117, 1952, pp. 447-484.

3. Steele, M. C., Liu, C. K., and Smith, J. O., "Critical Review and Interpretation of the Literature on Plastic (Inelastic) Behavior of Engineering Metallic Materials," Wright Air Development Center, WADC Technical Report 52-89, part 3, June, 1953.

4. Worley, Will J. and Breuer, Fred D., "Inelastic Behavior of Aluminum Alloy I-Beams with Elliptic-Type Web Section Cutouts," Wright Air Development Center, Report TR. 56-330, Pt. VII, August, 1957.

5. Worley, Will J., "Inelastic Behavior of Aluminum Alloy I-Beams with Elliptical Web Section Cutouts," Wright Air Development Center, Report TR. 56-330, Pt. V, October, 1956.

6. Worley, Will J. and Taira, Shuji, "Inelastic Behavior of Aluminum Alloy I-Beams with Rectangular Web Section Cutouts," Wright Air Development Center, Report TR. 56-330, Pt. II, April, 1956.

7. Worley, Will J. and Breuer, Fred D., "Elliptic-Type Closed Curves," *Product Engineering,* Vol. 28, No. 8, August, 1957, pp. 141-144.

8. "Alcoa Structural Handbook," Aluminum Company of America, Pittsburgh, Pennsylvania, 1955.

9. Shanley, F. R., "Applied Column Theory," *Transactions ASCE,* Vol. 115, 1950, pp. 698-750.

10. "Strength of Metal Aircraft Elements," ANC-5 Bulletin issued by the Department of the Air Force, Department of the Navy, Department of Commerce, March, 1955, pp. 86, 87.

11. Altfillisch, M. D., Cooke, B. R., and Toprac, A. A., "An Investigation of Welded Open-Web Expanded Beams," *Welding Research,* Vol. 22, No. 2, Feb. 1957, pp. 77-88.

18. Bibliography

Arranged in chronological order.

A. Cutouts

1. Kuhn, Paul, "Skin Stresses Around Inspection Cutouts," NACA, ARR, December, 1941.

2. Kuhn, Paul, "The Strength and Stiffness of Shear Webs with and without Lightening Holes," NACA Wartime Report, L-402, June, 1942.

3. Kuhn, Paul, "The Strength and Stiffness of Shear Webs with Round Lightening Holes Having 45° Flanges," NACA Wartime Report, L-323, December, 1942.

4. Leving, L. Ross, "Test of Beams Having Webs with Large Circular Lightening Holes," NACA, RB4B23 (WR L-524), Feb., 1944.

5. Nibs, Alfred S., "Elastic Properties of Channels with Unflanged Lightening Holes," NACA, TN 924, March, 1944.

6. Ruffner, B. F., and Schmidt, C. L., "Stresses at Cutouts in Shear Resistant Webs as Determined by the Photoelastic Method," NACA, TN 984, Oct., 1945.

7. Kuhn, Paul and Moggio, E. M., "Stresses Around Large Cut-outs in Torsion Boxes," NACA, TN 1066, May, 1946.

8. Hoff, N. J. and Boley, Bruno A., "Stresses in and General Instability of Monocoque Cylinders with Cutouts. I — Experimental Investigation of Cylinders with a Symmetric Cutout Subjected to Pure Bending," NACA, TN 1013, June, 1946.

9. Hoff, N. J., Boley, Bruno A., and Klein, Bertram, "Stresses in and General Instability of Monocoque Cylinders with Cutouts. II — Calculation of the Stresses in a Cylinder with a Symmetric Cutout," NACA, TN 1014, June, 1946.

10. Podorozhny, A. A., "Investigation of Behavior of Thin-Walled Panels with Cut-outs," NACA, TN 1094, Sept., 1946.

11. Hoff, N. J., Boley, Bruno A., and Klein, Bertram, "Stresses in and General Instability of Monocoque Cylinders with Cutouts. III-Calculation of the Buckling Load of Cylinders with Symmetric Cutout Subjected to Pure Bending," NACA, TN 1263, May, 1947.

12. Hoff, N. J., Kase, H., and Liebowitz, H., "Interaction Between the Spars of Semimonocoque Wings with Cut-outs," NACA, TN 1324, July, 1947.

13. Hoff, N. J. and Klein, Bertram, "Stresses in and General Instability of Monocoque Cylinders with Cutouts. V — Calculation of the Stresses in Cylinders with Side Cutout," NACA, TN 1435, Jan., 1948.

14. Hoff, N. J., Boley, Bruno A., and Viggiano, Louis R., "Stresses in and General Instability of Monocoque Cylinders with Cutouts. IV — Pure Bending Tests of Cylinders with Side Cutout," NACA, TN 1264, Feb., 1948.

15. Hoff, N. J., Klein, Bertram, and Boley, Bruno A., "Stresses in and General Instability of Monocoque Cylinders with Cutouts. VI — Calculation of the Buckling Load of Cylinders with Side Cutout Subjected to Pure Bending," NACA, TN 1436, March, 1948.

16. Ketter, Robert L., Keminsky, Edmond L., and Beedle, Lynn S., "Plastic Deformation of Wide-Flange Beam-Columns," *Proceedings ASCE,* Vol. 79, separate no. 330, Nov., 1953, 53 pages.

17. Masur, Ernest F., "Post-Buckling Strength of Redundant Trusses," *Transactions ASCE,* Vol. 119, 1954, pp. 699-712.

B. Vierendeel Trusses

18. Rucquoi, Leon G., "Vierendeel Truss Bridges Popular in Belgium," *Engineering News Record,* Vol. 115, July 25, 1935, pp. 116-118.

19. "Vierendeel Welded Trusses Used for Dutch Road Bridge," (editorial), *Engineering News Record,* Vol. 116, Jan. 2, 1936, p. 4.

20. Evans, L. T., "Vierendeel Girder Bridge Introduced in America," *Engineering News Record,* Vol. 117, Oct. 1, 1936, pp. 471-472.

21. Vierendeel, A., "Vierendeel Truss Bridges," *Engineering News Record,* Vol. 118, March 4, 1937, p. 345.

22. Young, Dana, "Analysis of Vierendeel Trusses," *Transactions ASCE,* Vol. 102, 1937, pp. 869-896, plus discussion, pp. 897-938.

23. Goldberg, J. E., "Analysis of Two Column Symmetrical Bents and Vierendeel Trusses Having Parallel and Equal Chord," *Proceedings, American Concrete Institute,* Vol. 44, Nov., 1947, pp. 225-234.

24. Courland, R. H., "One Story Vierendeel Trusses Ideally Suited to School Building," *Civil Engineering,* Vol. 22, Oct., 1952, pp. 56-60.

The Engineering Experiment Station was established by act of the University of Illinois Board of Trustees on December 8, 1903. Its purpose is to conduct engineering investigations that are important to the industrial interests of the state.

The management of the Station is vested in an Executive Staff composed of the Director, the Associate Director, the heads of the departments in the College of Engineering, the professor in charge of Chemical Engineering, and the Director of Engineering Information and Publication. This staff is responsible for establishing the general policies governing the work of the Station. All members of the College of Engineering teaching staff are encouraged to engage in the scientific research of the Station.

To make the results of its investigations available to the public, the Station publishes a series of bulletins. Occasionally it publishes circulars which may contain timely information compiled from various sources not readily accessible to the Station clientele or may contain important information obtained during the investigation of a particular research project but not having a direct bearing on it. A few reprints of articles appearing in the technical press and written by members of the staff are also published.

In ordering copies of these publications reference should be made to the Engineering Experiment Station Bulletin, Circular, or Reprint Series number which is at the upper left hand corner on the cover. Address

ENGINEERING PUBLICATIONS OFFICE
114 CIVIL ENGINEERING HALL
UNIVERSITY OF ILLINOIS
URBANA, ILLINOIS